arXiv:1107.4977v2 [astro-ph.CO] 31 Aug 2011

γ-RAY AND PARSEC-SCALE JET PROPERTIES OF A COMPLETE SAMPLE OF BLAZARS FROM THE MOJAVE PROGRAM

M. L. Lister[1], M. Aller[2], H. Aller[2], T. Hovatta[1,9], K. I. Kellermann[3], Y. Y. Kovalev[4,5], E. T. Meyer[6], A. B. Pushkarev[7,8,5], E. Ros[5,10] (for the MOJAVE collaboration) and M. Ackermann[11], E. Antolini[12,13], L. Baldini[14], J. Ballet[15], G. Barbiellini[16,17], D. Bastieri[18,19], K. Bechtol[11], R. Bellazzini[14], B. Berenji[11], R. D. Blandford[11], E. D. Bloom[11], M. Boeck[20,21], E. Bonamente[12,13], A. W. Borgland[11], J. Bregeon[14], M. Brigida[22,23], P. Bruel[24], R. Buehler[11], S. Buson[18,19], G. A. Caliandro[25], R. A. Cameron[11], P. A. Caraveo[26], J. M. Casandjian[15], E. Cavazzuti[27], C. Cecchi[12,13], C. S. Chang[28,5], E. Charles[11], A. Chekhtman[29], C. C. Cheung[30], J. Chiang[11], S. Ciprini[31,13], R. Claus[11], J. Cohen-Tanugi[32], J. Conrad[33,34,35], S. Cutini[27], F. de Palma[22,23], C. D. Dermer[36], E. do Couto e Silva[11], P. S. Drell[11], A. Drlica-Wagner[11], C. Favuzzi[22,23], S. J. Fegan[24], E. C. Ferrara[37], J. Finke[36], W. B. Focke[11], P. Fortin[24], Y. Fukazawa[38], P. Fusco[22,23], F. Gargano[23], D. Gasparrini[27], N. Gehrels[37], S. Germani[12,13], N. Giglietto[22,23], F. Giordano[22,23], M. Giroletti[39], T. Glanzman[11], G. Godfrey[11], I. A. Grenier[15], S. Guiriec[40], D. Hadasch[25], M. Hayashida[11], E. Hays[37], D. Horan[24], R. E. Hughes[41], G. Jóhannesson[42], A. S. Johnson[11], M. Kadler[43,20,44,45], H. Katagiri[46], J. Kataoka[47], J. Knödlseder[48,49], M. Kuss[14], J. Lande[11], F. Longo[16,17], F. Loparco[22,23], B. Lott[50], M. N. Lovellette[36], P. Lubrano[12,13], G. M. Madejski[11], M. N. Mazziotta[23], W. McConville[37,51], J. E. McEnery[37,51], J. Mehault[32], P. F. Michelson[11], T. Mizuno[38], C. Monte[22,23], M. E. Monzani[11], A. Morselli[52], I. V. Moskalenko[11], S. Murgia[11], M. Naumann-Godo[15], S. Nishino[38], P. L. Nolan[11], J. P. Norris[53], E. Nuss[32], M. Ohno[54], T. Ohsugi[55], A. Okumura[11,54], N. Omodei[11], E. Orlando[11,56], M. Ozaki[54], D. Paneque[57,11], D. Parent[58], M. Pesce-Rollins[14], M. Pierbattista[15], F. Piron[32], G. Pivato[19], S. Rainò[22,23], A. Readhead[59], A. Reimer[60,11], O. Reimer[60,11], J. L. Richards[59], S. Ritz[61], H. F.-W. Sadrozinski[61], C. Sgrò[14], M. S. Shaw[11], E. J. Siskind[62], G. Spandre[14], P. Spinelli[22,23], H. Takahashi[55], T. Tanaka[11], J. G. Thayer[11], J. B. Thayer[11], D. J. Thompson[37], G. Tosti[12,13], A. Tramacere[11,63,64], E. Troja[37,65], T. L. Usher[11], J. Vandenbroucke[11], V. Vasileiou[32], G. Vianello[11,63], V. Vitale[52,66], A. P. Waite[11], P. Wang[11], B. L. Winer[41], K. S. Wood[36], S. Zimmer[33,34] (for the *Fermi* LAT collaboration)

ABSTRACT

We investigate the *Fermi* LAT γ-ray and 15 GHz VLBA radio properties of a joint γ-ray- and radio-selected sample of AGNs obtained during the first 11 months of the *Fermi* mission (2008 Aug 4 - 2009 Jul 5). Our sample contains the brightest 173 AGNs in these bands above declination $-30°$ during this period, and thus probes the full range of γ-ray loudness (γ-ray to radio band luminosity ratio) in the bright blazar population. The latter quantity spans at least four orders of magnitude, reflecting a wide range of spectral energy distribution (SED) parameters in the bright blazar population. The BL Lac objects, however, display a linear correlation of increasing γ-ray loudness with synchrotron SED peak frequency, suggesting a universal SED shape for objects of this class. The synchrotron self-Compton model is favored for the γ-ray emission in these BL Lacs over external seed photon models, since the latter predict a dependence of Compton dominance on Doppler factor that would destroy any observed synchrotron SED peak - γ-ray loudness correlation. The high-synchrotron peaked (HSP) BL Lac objects are distinguished by lower than average radio core brightness temperatures, and none display large radio modulation indices or high linear core polarization levels. No equivalent trends are seen for the flat-spectrum radio quasars (FSRQ) in our sample. Given the association of such properties with relativistic beaming, we suggest that the HSP BL Lacs have generally lower Doppler factors than the lower-synchrotron peaked BL Lacs or FSRQs in our sample.

Subject headings: galaxies: active — galaxies: jets — radio continuum: galaxies — gamma rays: observations — quasars: general — BL Lacertae objects: general

[1] Department of Physics, Purdue University, 525 Northwestern Avenue, West Lafayette, IN 47907, USA; mlister@purdue.edu

[2] Department of Astronomy, University of Michigan, 817 Dennison Building, Ann Arbor, MI 48 109, USA;

[3] National Radio Astronomy Observatory, 520 Edgemont Road, Charlottesville, VA 22903, USA;

[4] Astro Space Center of Lebedev Physical Institute, Profsoyuznaya 84/32, 117997 Moscow, Russia;

[5] Max-Planck-Institut für Radioastronomie, Auf dem Hügel 69, 53121 Bonn, Germany;

[6] Department of Physics and Astronomy, Rice University, Houston, TX 77005

[7] Pulkovo Observatory, Pulkovskoe Chaussee 65/1, 196140 St. Petersburg, Russia;

[8] Crimean Astrophysical Observatory, 98409 Nauchny, Crimea, Ukraine;

[9] Owens Valley Radio Observatory, California Institute of Technology

[10] Departament d'Astronomia i Astrofísica, Universitat de València, E-

46100 Burjassot, Valéncia, Spain

[11] W. W. Hansen Experimental Physics Laboratory, Kavli Institute for Particle Astrophysics and Cosmology, Department of Physics and SLAC National Accelerator Laboratory, Stanford University, Stanford, CA 94305, USA

[12] Istituto Nazionale di Fisica Nucleare, Sezione di Perugia, I-06123 Perugia, Italy

[13] Dipartimento di Fisica, Università degli Studi di Perugia, I-06123 Perugia, Italy

[14] Istituto Nazionale di Fisica Nucleare, Sezione di Pisa, I-56127 Pisa, Italy

[15] Laboratoire AIM, CEA-IRFU/CNRS/Université Paris Diderot, Service d'Astrophysique, CEA Saclay, 91191 Gif sur Yvette, France

[16] Istituto Nazionale di Fisica Nucleare, Sezione di Trieste, I-34127 Trieste, Italy

[17] Dipartimento di Fisica, Università di Trieste, I-34127 Trieste, Italy

[18] Istituto Nazionale di Fisica Nucleare, Sezione di Padova, I-35131

1. INTRODUCTION

The successful launch of the *Fermi Gamma-Ray Space Telescope* in 2008 has brought about a new era in our understanding of blazars, which dominate the extragalactic sky at high energies. Because of their highly variable fluxes and spectral energy distributions (SEDs), blazar samples are typically subject to large biases, making it difficult to study their demographics. With the nearly continuous all-sky monitoring

capabilities of *Fermi's* Large Area Telescope (LAT), however, it is now possible to construct well-defined samples that can be used to investigate the wide range of jet properties in these powerful AGNs (e.g., Abdo et al. 2010d; Kovalev 2009).

One of these properties that has been of considerable interest since the era of the *Compton Gamma Ray Observatory* (CGRO) in the 1990s is γ-ray loudness, or in other words, why only a particular small subset of known AGNs (~ 100; Hartman et al. 1999) were detected by the CGRO's EGRET telescope. Considerable evidence has been presented by many researchers (e.g., Dondi & Ghisellini 1995; Kellermann et al. 2004; Kovalev et al. 2005; Jorstad et al. 2001; Taylor et al. 2007) supporting the idea that relativistic Doppler boosting has a large impact on AGN γ-ray emission, but lingering questions regarding the roles of the flaring duty cycle and the AGN spectral energy distribution remain. The superior sensitivity and full-time survey operation mode of *Fermi* has now provided substantial insight into these issues. With the release of the 1FGL catalog (Abdo et al. 2010a), the strong impact of SED characteristics on the fainter γ-ray AGN population was realized, as the sky at these levels becomes dominated by high-synchrotron peaked BL Lac objects. At the same time, the predominant association of *Fermi* LAT sources with flat-spectrum radio quasars (FSRQ) and BL Lacs (blazars) has established Doppler boosting as the primary factor in determining γ-ray loudness in the brightest AGNs.

In this paper, we follow up on previous analyses of bright blazars that were based on the initial 3 month LAT data set presented by Abdo et al. (2009). These studies established several important AGN radio/γ-ray connections using quasi-simultaneous VLBA observations, namely that the γ-ray photon flux correlates with the parsec scale radio flux density (Kovalev et al. 2009; Arshakian et al. 2011), and that the jets of the LAT-detected blazars have higher-than-average apparent speeds (Lister et al. 2009a), larger apparent opening angles (Pushkarev et al. 2009), more compact radio cores (Kovalev et al. 2009), strong polarization near the base of the jet (Linford et al. 2011), and higher variability Doppler factors (Savolainen et al. 2010). In addition, AGN jets have

Padova, Italy

[19] Dipartimento di Fisica "G. Galilei", Università di Padova, I-35131 Padova, Italy

[20] Dr. Remeis-Sternwarte Bamberg & ECAP, Sternwartstrasse 7, D-96049 Bamberg, Germany

[21] email: moritz.boeck@sternwarte.uni-erlangen.de

[22] Dipartimento di Fisica "M. Merlin" dell'Università e del Politecnico di Bari, I-70126 Bari, Italy

[23] Istituto Nazionale di Fisica Nucleare, Sezione di Bari, 70126 Bari, Italy

[24] Laboratoire Leprince-Ringuet, École polytechnique, CNRS/IN2P3, Palaiseau, France

[25] Institut de Ciències de l'Espai (IEEE-CSIC), Campus UAB, 08193 Barcelona, Spain

[26] INAF-Istituto di Astrofisica Spaziale e Fisica Cosmica, I-20133 Milano, Italy

[27] Agenzia Spaziale Italiana (ASI) Science Data Center, I-00044 Frascati (Roma), Italy

[28] Institut de Radioastronomie Millimétrique, 300 Rue de la Piscine, Domaine Universitaire, 38406 Saint Martin d'Héres, France

[29] Artep Inc., 2922 Excelsior Springs Court, Ellicott City, MD 21042, resident at Naval Research Laboratory, Washington, DC 20375

[30] National Research Council Research Associate, National Academy of Sciences, Washington, DC 20001, resident at Naval Research Laboratory, Washington, DC 20375

[31] ASI Science Data Center, I-00044 Frascati (Roma), Italy

[32] Laboratoire Univers et Particules de Montpellier, Université Montpellier 2, CNRS/IN2P3, Montpellier, France

[33] Department of Physics, Stockholm University, AlbaNova, SE-106 91 Stockholm, Sweden

[34] The Oskar Klein Centre for Cosmoparticle Physics, AlbaNova, SE-106 91 Stockholm, Sweden

[35] Royal Swedish Academy of Sciences Research Fellow, funded by a grant from the K. A. Wallenberg Foundation

[36] Space Science Division, Naval Research Laboratory, Washington, DC 20375-5352

[37] NASA Goddard Space Flight Center, Greenbelt, MD 20771, USA

[38] Department of Physical Sciences, Hiroshima University, Higashi-Hiroshima, Hiroshima 739-8526, Japan

[39] INAF Istituto di Radioastronomia, 40129 Bologna, Italy

[40] Center for Space Plasma and Aeronomic Research (CSPAR), University of Alabama in Huntsville, Huntsville, AL 35899

[41] Department of Physics, Center for Cosmology and Astro-Particle Physics, The Ohio State University, Columbus, OH 43210, USA

[42] Science Institute, University of Iceland, IS-107 Reykjavik, Iceland

[43] Institut für Theoretische Physik and Astrophysik, Universität Würzburg, D-97074 Würzburg, Germany

[44] Universities Space Research Association (USRA), Columbia, MD 21044, USA

[45] Center for Research and Exploration in Space Science and Technology (CRESST) and NASA Goddard Space Flight Center, Greenbelt, MD 20771

[46] College of Science , Ibaraki University, 2-1-1, Bunkyo, Mito 310-8512, Japan

[47] Research Institute for Science and Engineering, Waseda University, 3-4-1, Okubo, Shinjuku, Tokyo 169-8555, Japan

[48] CNRS, IRAP, F-31028 Toulouse cedex 4, France

[49] GAHEC, Université de Toulouse, UPS-OMP, IRAP, Toulouse, France

[50] Université Bordeaux 1, CNRS/IN2p3, Centre d'Études Nucléaires de Bordeaux Gradignan, 33175 Gradignan, France

[51] Department of Physics and Department of Astronomy, University of Maryland, College Park, MD 20742

[52] Istituto Nazionale di Fisica Nucleare, Sezione di Roma "Tor Vergata", I-00133 Roma, Italy

[53] Department of Physics, Boise State University, Boise, ID 83725, USA

[54] Institute of Space and Astronautical Science, JAXA, 3-1-1 Yoshinodai, Chuo-ku, Sagamihara, Kanagawa 252-5210, Japan

[55] Hiroshima Astrophysical Science Center, Hiroshima University, Higashi-Hiroshima, Hiroshima 739-8526, Japan

[56] Max-Planck Institut für extraterrestrische Physik, 85748 Garching, Germany

[57] Max-Planck-Institut für Physik, D-80805 München, Germany

[58] Center for Earth Observing and Space Research, College of Science, George Mason University, Fairfax, VA 22030, resident at Naval Research Laboratory, Washington, DC 20375

[59] Cahill Center for Astronomy and Astrophysics, California Institute of Technology, Pasadena, CA 91125

[60] Institut für Astro- und Teilchenphysik and Institut für Theoretische Physik, Leopold-Franzens-Universität Innsbruck, A-6020 Innsbruck, Austria

[61] Santa Cruz Institute for Particle Physics, Department of Physics and Department of Astronomy and Astrophysics, University of California at Santa Cruz, Santa Cruz, CA 95064, USA

[62] NYCB Real-Time Computing Inc., Lattingtown, NY 11560-1025, USA

[63] Consorzio Interuniversitario per la Fisica Spaziale (CIFS), I-10133 Torino, Italy

[64] INTEGRAL Science Data Centre, CH-1290 Versoix, Switzerland

[65] NASA Postdoctoral Program Fellow, USA

[66] Dipartimento di Fisica, Università di Roma "Tor Vergata", I-00133 Roma, Italy

been found to be in a more active radio state within several months of the LAT-detection of their strong γ-ray emission (Kovalev et al. 2009), which was subsequently confirmed by Pushkarev et al. (2010).

With the release of the 1st LAT AGN catalog (1LAC; Abdo et al. 2010d) based on the initial 11 months of *Fermi* data, it is now possible to investigate the impact of Doppler beaming and SED characteristics on AGN γ-ray loudness using larger, more complete samples and better statistics. Here we present a joint analysis of *Fermi* and VLBA 15 GHz radio properties of the brightest radio and γ-ray AGN in the northern sky, based on data from the LAT instrument, flux density measurements from the OVRO and UMRAO radio observatories, and the MOJAVE VLBA program (Lister et al. 2009b). In particular we examine the differences in the SED and γ-ray properties of BL Lac objects with respect to FSRQs, and the relative role of relativistic beaming on their γ-ray loudness. Several complementary studies will examine the connection between γ-ray emission and superluminal speeds (Kadler et al., in prep.), detailed SED parameters (Chang et al., in prep.), and radio jet activity level (Lister et al., in prep.).

Throughout this paper, we use a ΛCDM cosmological model with $H_0 = 71$ km s^{-1} Mpc^{-1}, $\Omega_m = 0.27$, and $\Omega_\Lambda = 0.73$ (Komatsu et al. 2009).

2. SAMPLE SELECTION

2.1. *The MOJAVE Survey*

Beginning in 2002, we undertook in anticipation of the *Fermi* mission a program (MOJAVE: Lister & Homan 2005; Lister et al. 2009c) to assemble the most complete sample possible of bright AGNs that could be observed relatively easily on a regular basis with the VLBA. This meant choosing radio sources located in the northern sky that were bright enough for direct fringe detection on short integration times. Many of these had been observed regularly for up to seven years by the preceding VLBA 2 cm Survey program (Kellermann et al. 1998). Because of its lack of short interferometric baselines, the VLBA effectively filters out diffuse radio lobe emission, guaranteeing that this sample would be dominated by AGNs with bright, compact radio cores. As a further discriminator against steep-spectrum diffuse radio emission, we carried out the selection at a relatively high radio frequency (15 GHz).

Unlike blazar surveys in the optical or soft X-ray regimes, the radio emission from the brightest radio-loud blazars is not substantially obscured by or blended with emission from the host galaxy. Our VLBA-selected sample thus provides a relatively "clean" blazar sample, namely, one selected solely on the basis of beamed synchrotron emission from the relativistic jets.

In order to ensure a high overlap with *Fermi* and other blazar samples, we included in our MOJAVE monitoring program all blazars down to a specified radio flux density limit. The use of a lower flux-density cutoff in astronomical surveys is often dictated by practical concerns such as detector sensitivity or available observing time, but it also an important parameter in luminosity function and source population studies. A well-known downside is the introduction of a luminosity (Malmquist) bias, in which the average luminosity of sources in the flux-limited sample increases with redshift. Well-defined flux density limits are essential in blazar population studies, where the same objects are typically sampled in a variety of surveys at different wavelengths. With blazars also

comes the difficulty of substantial flux and spectral variability. Considerable challenges arise when attempting to compare data from different wavelength surveys that are not cotemporaneous, especially when each individual survey may contain or omit certain objects depending on their activity state at the time the survey was made.

We addressed the issue of flux variability in MOJAVE by considering a wide time window during which any source that exceeded the flux limit was included in the sample. Although this can potentially introduce a different kind of bias towards highly flaring sources, it has been effectively used in the 1FGL catalog (Abdo et al. 2010a) and in previous radio blazar surveys (e.g., Wehrle et al. 1992, Valtaoja et al. 1992). It generally requires a large set of well-sampled flux density monitoring data. Fortunately we had a large archive of VLBA (from the 2 cm Survey) and single-dish (from UM-RAO and RATAN) radio flux density measurements of bright AGN ranging from 1994.0 to 2004.0, from which we constructed the original MOJAVE sample. Any AGN with declination above $-20°$ with measured or inferred 15 GHz VLBA density that exceeded 1.5 Jy (2 Jy for declinations $< 0°$) during this period was included (see Lister et al. 2009b and the MOJAVE website[67]). In order to obtain an even larger overlap with *Fermi* , we have since extended the MOJAVE sample to include all sources above 1.5 Jy north of declination $-30°$ for all epochs from 1994.0 to the present. It is from this extended survey that we draw the radio-matching sample used in this paper (§ 2.3).

2.2. *The 1FM γ-ray-Selected Sample*

In assembling our γ-ray AGN sample for this paper, our main considerations were that the sources needed to be suitably bright at γ-ray energies, and have sufficiently strong compact radio emission for imaging with the VLBA. We also required the sample to be of reasonable size (~ 100 sources) to ensure good statistics, yet small enough so that it could still be fully monitored by the MOJAVE VLBA program. We began by eliminating from the LAT 1FGL catalog (Abdo et al. 2010a) all of the γ-ray sources known to be associated with non-extragalactic objects, as well as one gravitationally lensed AGN (MG J0221+3555 = 1FGL J0221.0+3555). We also excluded five millisecond γ-ray pulsars recognized after the publication of the 1LAC (Abdo et al. 2010d) and 1FGL (Abdo et al. 2010a) papers: 1FGL J1231.1−1410 & 1FGL J2214.8+3002 (Ransom et al. 2011), 1FGL J2017.3+0603 & 1FGL J2302.8+4443 (Cognard et al. 2011), and 1FGL J2043.2+1709 (Abdo et al. 2011).

The specific selection criteria for our initial candidate γ-ray-limited sample were:

- average integrated > 0.1 GeV energy flux $\geq 3 \times 10^{-11}$ erg cm^{-2} s^{-1} between 2008 Aug 4 and 2009 Jul 5.

- J2000 declination $> -30°$

- Galactic latitude $|b| > 10°$

- not associated with a Galactic source or gravitational lens

These criteria yielded a total of 118 candidate AGNs. We note that the subsequently published 1st LAT AGN Catalog
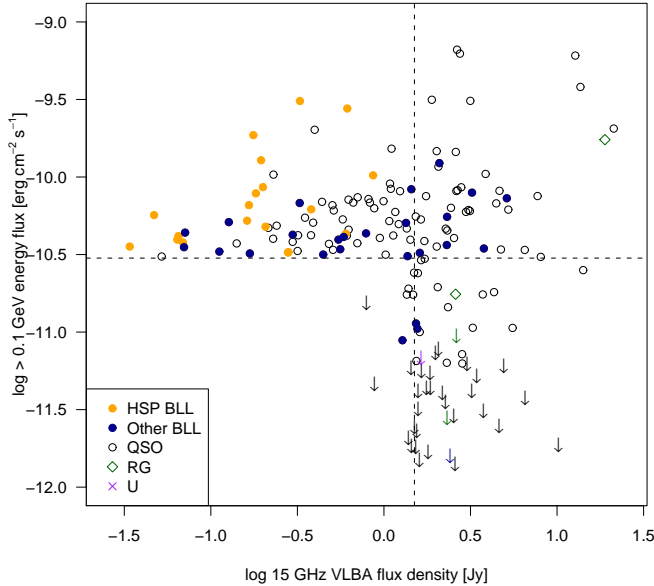
Figure 1. Plot of 11 month *Fermi* average > 0.1 GeV energy flux versus 15 GHz VLBA flux density for our joint AGN sample. The filled circles represent BL Lac objects, with the high synchrotron peaked ones in orange and others in blue. The open circles represent quasars, the green diamonds radio galaxies, and the purple crosses optically unidentified objects. Upper limits on the γ-ray fluxes are indicated by arrows. All of the BL Lac objects are detected by the LAT, with the exception of J0006−0623. The vertical dashed line indicates the sample radio limit of 1.5 Jy, and the horizontal dashed line indicates the γ-ray limit of 3×10^{-11} erg cm^{-2} s^{-1}. Note that the radio flux density data correspond to either a median or "reference" epoch coincident with our VLBA observations (see § 3.1), and do not necessarily coincide with the epoch of maximum radio flux density during the 11 month LAT period. Some AGNs in the bottom left quadrant thus have plotted flux densities below 1.5 Jy.

(1LAC; Abdo et al. 2010d) listed some additional AGN associations for some 1FGL sources that were not given in the Abdo et al. (2010a) 1FGL catalog. We used these new associations to construct our 1FGL-MOJAVE (hereafter 1FM) candidate list. In the case of three bright γ-ray sources which had more than one unique AGN association: 1FGL J0339.2−0143, 1FGL J0442.7−0019, 1FGL J1130.2−1447, we assumed they were associated with the very bright, compact FSRQs J0339−0146, J0442−0017, and J1130−1449, respectively.

For the sky region criteria, we used the position of the radio source in cases where an AGN association existed, and the LAT position otherwise. Of the 1FGL sources that met our criteria, only two had no clear radio source association. On 2009 Dec 30 and 2009 Dec 31 we obtained 15 GHz radio telescope pointings at OVRO at the LAT coordinates of these sources, which yielded 0.11 Jy for 1FGL J1653.6−0158, and an upper limit of 0.01 Jy for 1FGL J2339.7−0531. Since there were numerous possible faint radio counterparts in the LAT error circle (as seen in NVSS images, Condon et al. 1998), we dropped these two LAT sources from the 1FM sample. We subsequently found that all of the remaining 116 candidate AGNs were bright enough for direct imaging by the VLBA at 15 GHz (see § 3.2). These formed our 1FM γ-ray limited sample (Table 1).

2.3. *The 1FM-Matching Radio-Selected Sample*

For the purposes of constructing a matching radio-selected sample, we used the same sky region criteria as the 1FM, this

Table 1
AGN Samples

Sample	N_{tot}	N_{FSRQ}	N_{BLL}
Combined sample	173	123	45 (17)
γ-ray-selected (1FM)	116	74	41 (17)
Radio-selected	105	86	14 (0)
Common to both samples	48	37	10 (0)

Note. — N_{tot} = total number of AGNs, N_{FSRQ} = total number of flat-spectrum radio quasars, N_{BLL} = total number of BL Lac objects (number of which are known to be high-spectral peaked).

time choosing all AGNs known to have exceeded $S_{VLBA} = 1.5$ Jy at 15 GHz during the initial *Fermi* 11 month period, without regards to γ-ray flux. To carry out this selection, we relied on MOJAVE VLBA measurements, as well as OVRO and UMRAO single-dish data, from which compact (VLBA) flux densities could be estimated (§3.1). There are 105 AGNs in our final 1FM matching radio-selected sample, 48 of which are also in the 1FM γ-ray-selected sample. In Figure 1 we plot the 11-month > 0.1 GeV average γ-ray energy flux versus 15 GHz VLBA flux density, which shows the region of the flux-flux density plane covered by our survey. We note that the radio flux density data plotted in Figure 1 correspond to either a median or "reference" epoch coincident with our VLBA observations (see § 3.1), and do not necessarily coincide with the epoch of maximum radio flux density during the 11 month LAT period. Thus, some AGNs in the radio-selected sample have plotted flux densities below 1.5 Jy.

2.4. *Selection Biases*

We have assembled two complete samples of the brightest AGNs in the northern γ-ray and radio sky, as seen during the first 11 months of the *Fermi* mission. We list their general properties in Table 2. The optical redshifts and classifications are from the compilations of Lister et al. (2009b) and NED (see Appendix for notes on individual sources). Note that we classify J0238+1636 as a quasar because of its occasional broad emission lines (Raiteri et al. 2007), and the presence of a break in its γ-ray spectrum that is characteristic of FSRQs (Abdo et al. 2010c). For the purposes of this paper, we have grouped two narrow-line Seyfert 1 galaxies J0948+0022 and J1504+1029 (Foschini 2011) with the quasar class.

The SED data are taken mainly from Chang (2010), Abdo et al. (2010e), and other papers in the literature as indicated in column 8. We use the following nomenclature for high-, intermediate- and low-synchrotron peaked blazars: LSP $< 10^{14}$, $10^{14} <$ ISP $< 10^{15}$, and HSP $> 10^{15}$, where the values refer to the synchrotron SED peak frequency ν_s in Hz.

Although our γ-ray and radio selections are both made on the basis of compact beamed jet emission, there is only a 28% overlap in the two samples. This is perhaps lower than might be expected, given the strong correlations previously seen between the 1LAC catalog and flat-spectrum radio sources (Abdo et al. 2010d). As we discuss in § 3.3, however, this is mainly a consequence of the wide range of γ-ray loudness in the bright blazar population. There is also some likelihood that any particular AGN will not have a LAT association because it happens to lie in a confused region that contains several bright γ-ray sources, or has a high diffuse γ-ray background. The latter case is less likely to occur however for

the bright non-Galactic-plane sources we are considering. We have carefully examined our candidate list and found only one possible case of a missed association: 1FGL J1642.5+3947. Recent analysis by the LAT team (Schinzel et al. 2010) has led us to associate this source with the FSRQ J1642+3948 (3C 345).

The nature of our γ-ray sample selection differs from that of our radio sample, since it uses average fluxes instead of maximum measured flux densities, and it spans a wide energy band compared to the radio. It is thus more sensitive to the shapes of the AGN SEDs, which can have curvature and breaks within the LAT detector band. The spectral response function of the LAT detector and its favoritism towards harder sources causes some selection bias towards faint high-synchrotron peaked AGNs (Abdo et al. 2010a). We note, however, that the sources in our 1FM sample are selected well above the instrument sensitivity level of the LAT detector, and should be devoid of biases related to threshold effects.

The above selection biases do not have a large impact on the analysis presented in this paper, since our primary goal is to identify broad statistical trends between the γ-ray emission and radio jet properties. For this purpose a representative blazar sample that spans a wide range of SED peak frequency and γ-ray loudness is appropriate. Future studies using more extensive *Fermi* data will address these issues in considerably more detail, with better statistics. These will be needed for accurate determination of the blazar γ-ray luminosity function for different redshift ranges and optical sub-classes.

3. OBSERVATIONAL DATA

3.1. *Radio Flux Density Data*

We list the radio flux density data for our sample in Table 3. For each AGN we selected a VLBA "reference" epoch, which was chosen to be the closest MOJAVE VLBA observation to the end of the initial 11-month *Fermi* period. In the case of 41 sources, no VLBA data were available within this period, so we used the first available MOJAVE VLBA epoch following this period. The latter epoch dates ranged from 2009 July 23 to 2010 Nov 29. We list the reference epoch dates and total 15 GHz VLBA flux densities in columns 3 and 4, respectively. In column 5 we list the median single dish flux density from OVRO at 15 GHz (or 14.5 GHz at UMRAO as indicated) during the same 11 month period (Richards et al. 2011; Aller et al. 2003).

The vast majority of the radio sources in our sample are strongly core dominated at 15 GHz (Lister et al. 2009b), and therefore there is typically very little flux density that is missed by the VLBA. In order to estimate this amount for each source, we compared our historical MOJAVE flux density measurements with cotemporeaneous 14.5 GHz UMRAO measurements (within 7 days), and 15 GHz OVRO measurements that were interpolated to the VLBA epoch date. By taking the mean of these single dish-minus-VLBA flux density measurements, we obtained the extended flux density values that are tabulated in column 6. For the sources with no value listed, the amount of extended flux density was smaller than 3 times the associated measurement error. The errors in our VLBA flux density measurements are on the order of 5%, while the single-dish errors are smaller (Richards et al. 2011; Aller et al. 2003).

For the purposes of determining an average γ-ray loudness parameter G_r for each source during the first 11 months of LAT science operations (Section 3.3), we required an esti-

mate of the median 15 GHz VLBA radio flux density during the initial 11-month *Fermi* period. Since the single dish radio monitoring data were much more densely sampled than the VLBA data, we estimated the latter by using the single dish median in column 5 of Table 3 and subtracting the source's extended flux density (assuming zero extended flux density for those sources with no value listed in column 6). For 28 sources which lacked a single dish median value, we used the VLBA flux density at the reference epoch (column 4).

We also collected radio variability statistics for 84% of our AGN sample using 15 GHz OVRO observatory data taken during the first 11 months of the *Fermi* mission. The modulation index data are described and tabulated by Richards et al. (2011). This index is defined as the standard deviation of the flux density measurements in units of the mean measured flux density (e.g., Quirrenbach et al. 2000), and is less sensitive to outlier data points than other variability measures.

3.2. *VLBA Data*

The 15 GHz radio VLBA data were obtained as part of the MOJAVE observing program (Lister et al. 2009b), and consist of linear polarization and total intensity images with a typical image FWHM restoring beam of approximately 1 milliarcsecond. This corresponds to a scale of a few parsecs at the typical redshifts ($z \simeq 1$) of our sample AGNs. We obtained fractional linear polarization and electric vector position angle measurements for the reference epoch image using the methods described by Lister & Homan (2005). We calculated the mean position angle of each jet on the sky by taking a flux density-weighted average of the position angles of all Gaussian jet components fit to all available 15 GHz VLBA epochs up to the end of 2010 in the MOJAVE archive. A description of the Gaussian model fitting method is given by Lister et al. (2009c). We used the Gaussian fit to the flat-spectrum core component of each jet at the VLBA reference epoch to determine a rest frame core brightness temperature T_b (column 5 of Table 4) for each jet according to

$$T_b = 1.222 \times 10^{12} \, \frac{S_{\text{core}} \, (1+z)}{\nu^2 \, \theta_{\text{maj}} \, \theta_{\text{min}}} \qquad \text{K,} \qquad (1)$$

where S_{core} is the fitted core flux density in Janskys at $\nu = 15$ GHz, and θ_{maj} and θ_{min} are the FWHM dimensions of the fitted elliptical Gaussian core components along the major and minor axes, respectively, in milliarcseconds. In cases where the best fit to the core was a zero-size (point) component, we used the signal-to-noise ratio formula of Kovalev et al. (2005) to determine a lower limit on T_b. For the 26 sources without a redshift we assumed $z = 0.3$ in calculating T_b (and G_r in Section 3.3), since most of these are BL Lac objects, and this corresponds to the median BL Lac redshift in our sample.

We obtained pc-scale jet opening angle measurements (as projected on the sky) using the method described by Pushkarev et al. (2009). We used a stacked image of all available 15 GHz epochs in the MOJAVE archive for this purpose. The median opening angle value for each jet is listed in Table 4. Five γ-ray-selected sources with weak radio flux densities (< 200 mJy) did not possess sufficiently bright jet emission to estimate their opening angles. These were J0136+3906, J0507+6737, J1037+5711, J1303+2433, and J1725+1152. Additionally, the FSRQ J0957+5522 (4C +55.17) is largely resolved by the the long baselines of the VLBA at 15 GHz and thus has a low brightness temperature and very little measurable jet structure (McConville et al.

2011; Rossetti et al. 2005). Our opening angle measurements based on the stacked-epoch images are in generally good agreement with the single-epoch measurements of the same sources by Pushkarev et al. (2009). In some sources our measured opening angle was much wider, because of the presence of low-brightness jet emission that was below the noise level in the single-epoch image. In a few other cases, the ejections of new moving jet features along different position angles over time resulted in a wider apparent opening angle than seen in the single-epoch image.

3.3. γ-ray Loudness

Our chosen statistic for describing γ-ray loudness is the ratio of average γ-ray luminosity during the first 11 months of the *Fermi* mission to the median 15 GHz VLBA radio luminosity. We have compiled this ratio G_r for all the AGNs in our sample using the 1FGL > 0.1 GeV γ-ray energy flux measurements of Abdo et al. (2010a) and the radio data described in § 3.1. These ratios are listed in Table 3.

In the 1FGL catalog, the γ-ray source significance is measured in terms of the Test Statistic (TS), where TS is defined as 2 times the difference in the log(likelihood) measure with and without the source included (Mattox et al. 1996). All sources in the 1FGL and 1LAC catalogs have TS > 25. For the 1FM radio-matching sources that had no associations in the 1LAC catalog, we determined an upper limit on the > 0.1 GeV photon flux directly from the 11-month *Fermi* LAT data, assuming a point source with a power law spectrum. We analyzed photons of the 'diffuse" class with a zenith angle smaller than $105°$ in the energy range 0.1–100 GeV within a circular region of interest (RoI) with a radius of $12°$ centered around the radio position of the source. We modeled the γ-ray emission from the RoI using extended Galactic and isotropic templates and all sources from the 1FGL catalog. We let the model parameters of sources in the RoI vary, and froze those of the outer sources to the catalog values. We used the standard *Fermi*-LAT *ScienceTools* software package (version v9r16p1) with the instrument response functions 'P6_V3_DIFFUSE" to obtain a flux value for each source. To obtain the upper limits we increased the flux from the maximum-likelihood value until $2\Delta \log(\text{likelihood}) = 4$ (Rolke et al. 2005). Our final upper limits thus correspond to $\sim 2\sigma$. For sources with TS < 1 we calculated a 95% upper limit using a Bayesian approach (Helene 1983). We converted these to energy fluxes according to

$$S_{0.1} = \frac{(\Gamma - 1)\, C_1\, E_1\, F_{0.1}}{(\Gamma - 2)} \left[1 - \left(\frac{E_1}{E_2}\right)^{\Gamma - 2} \right] \qquad \text{erg cm}^{-2}\,\text{s}^{-1}, \tag{2}$$

where $F_{0.1}$ is the upper limit on the photon flux above $E_1 = 0.1$ GeV in photons cm^{-2} s^{-1}, $E_2 = 100$ GeV, and $C_1 = 1.602 \times 10^{-3}$ erg GeV^{-1}. In calculating these upper limits, we fixed the photon spectral index to $\Gamma = 2.1$.

We converted the measured energy fluxes and upper limits to γ-ray luminosities according to

$$L_\gamma = \frac{4\pi D_L^2\, S_{0.1}}{(1+z)^{2-\Gamma}} \qquad \text{erg s}^{-1}, \tag{3}$$

where D_L is the luminosity distance in cm, Γ is the 11-month average γ-ray photon spectral index for sources with 1LAC associations and $\Gamma = 2.1$ otherwise, z is the redshift, and $S_{0.1}$ is the 11-month average energy flux (or upper limit) above 0.1 GeV in erg cm^{-2} s^{-1}.
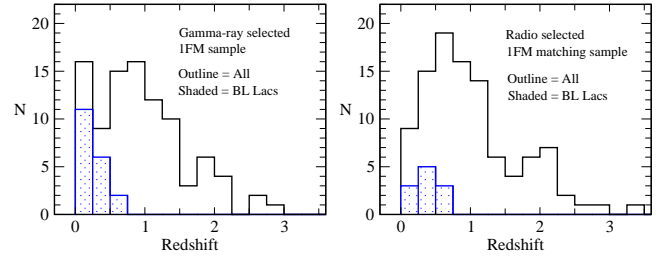
Figure 2. Left panel: redshift distribution of the γ-ray-selected 1FM sample. The full sample is represented by the solid line, and the BL Lac objects are shaded. There is one radio galaxy (J0319+4130 = 3C 84) at $z = 0.0176$. Right panel: redshift distribution for the radio-selected 1FM matching sample. There are four radio galaxies in the sample, all in the first ($z < 0.25$) bin.

As discussed by Abdo et al. (2010a), the lower-energy LAT band photon fluxes are poorly determined; therefore the energy flux over the full band is better defined than the 0.1 to 100 GeV photon flux. The average 11-month energy fluxes tabulated by Abdo et al. (2010a) were found by summing the energy fluxes in five individual bands over this energy range.

We calculated the radio luminosities over a 15 GHz wide bandwidth according to:

$$L_R = \frac{4\pi\, D_L^2\, \nu\, S_\nu}{(1+z)} \qquad \text{erg s}^{-1}, \tag{4}$$

where S_ν is the median VLBA flux density at $\nu = 15$ GHz as defined in § 3.1. We assumed a flat radio spectral index ($\alpha = 0$) for the purposes of the k-correction and luminosity calculations.

4. DATA ANALYSIS AND DISCUSSION

4.1. *Redshift Distributions*

The redshift data on our AGNs are incomplete (see Appendix), with missing values for 4 sources in the radio-selected sample, and 22 sources in the γ-ray-selected sample (the sources J0050−0929 and J0818+4222 are common to both samples). In Figure 2 we plot the redshift distributions for our samples. The redshifts range from $z = 0.00436$ to $z = 3.396$, and the distributions are generally peaked between $z = 0.5$ and $z = 1$. Kolmogorov-Smirnov (K-S) tests do not reject the null hypothesis that the γ-ray-selected and radio-selected samples are drawn from the same parent redshift distribution, even when the sources in common to both samples are excluded (D = 0.20, probability = 0.27). We find no statistical differences in the redshift distributions of the non-LAT detected versus LAT-detected AGNs in the combined samples (D = 0.16, probability = 0.49).

With respect to the redshifts of the quasars in the two samples, the K-S test suggests a marginal statistical difference in their distributions (D = 0.079, probability = 0.96). There are an insufficient number of radio galaxies to perform any statistical tests on them (there are 4 in the radio-selected sample; one of these is also in the γ-ray-selected sample). The overall redshift distribution of the γ-ray-selected sample has an additional peak at low redshift, due to the presence of at least 9 high synchrotron peaked (HSP) BL Lacs that are not in the radio selected sample (8 additional HSP BL Lacs lack redshift information). These objects also bring the overall fraction of BL Lacs up to 35% in the γ-ray-selected sample, as compared to only 13% for the radio-selected sample.

Because of the similarities in the properties and redshift distributions of the γ-ray and radio-selected samples, for the re-
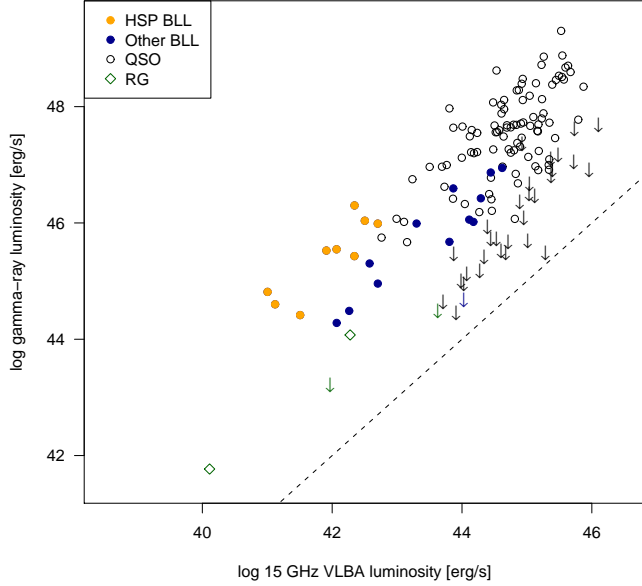
Figure 3. Plot of average γ-ray luminosity versus median VLBA 15 GHz radio luminosity. The filled circles represent BL Lac objects, with the high synchrotron peaked ones in orange and others in blue. The open circles represent quasars and the green diamonds radio galaxies. The arrows represent upper limits based on the 11-month LAT data. The dashed line represents the 1:1 luminosity ratio line.

Figure 4. Distribution of γ-ray to radio luminosity ratio for BL Lacs (top panel) and quasars (bottom panel). Upper limit values for AGNs with no *Fermi* 1LAC catalog associations are indicated by the dashed lines.

mainder of this paper we will no longer distinguish between them, referring instead to the joint sample of 173 AGNs.

4.2. γ-ray Loudness and Synchrotron Peak Frequency

A primary goal of our study is to examine the range of γ-ray loudness (G_r) present in the bright blazar population, and its dependence on other AGN jet properties. Since we have obtained data in several complete regions of the γ-ray-radio plane (i.e., γ-ray-bright/radio-faint; γ-ray-faint/radio-bright; γ-ray-bright/radio-bright) we can be assured of sampling the largest possible range of G_r in the brightest northern-sky blazars. Future studies of the γ-ray-weak/radio-weak region will be important for verifying whether the trends we identify here extend to the fainter blazar population.

In Figure 3 we plot γ-ray luminosity against 15 GHz VLBA luminosity. Despite our use of an average γ-ray luminosity over an 11-month period, the linear relationship for the non-censored data has only moderate scatter (0.6 dex). A linear regression fit to the non-censored data yields $\log L_\gamma = (0.92 \pm 0.05) \log L_R + 6.4 \pm 2$. The G_r values, which reflect the perpendicular distance of the data points from the dashed 1:1 line, span nearly 4 orders of magnitude, from below 3 to ∼ 15000. A clear division between the HSP and lower-synchrotron-peaked BL Lacs is evident, with the former having higher γ-ray loudness ratios.

None of the radio galaxies are significantly γ-ray-loud, with ratios all below 65. The quasars and BL Lacs have significantly different G_r distributions (Figure 4), with the former peaking at $G_r \simeq 10^3$ and the latter peaking above $10^{3.5}$. There is a substantial population of quasars with G_r values below 100, while all of the BL Lacs (with the exception of J0006−0623) have *Fermi* associations and $G_r > 60$. The Peto and Peto modification of Gehan's Wilcoxon two-sample test for censored data rejects the null hypothesis that the quasar and BL Lac G_r values come from the same parent population at the 99.99% confidence level.
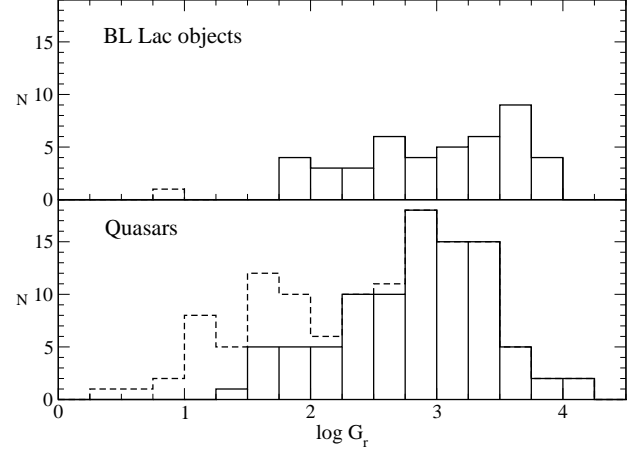
These differences are reflected in Figure 5, which shows γ-ray loudness plotted against the synchrotron SED peak frequency. The BL Lacs show a roughly linear correlation of the form $\log G_r = (0.40 \pm 0.06) \log \nu_s - 2.9 \pm 0.9$, with a scatter of 0.5 dex, while the quasars show no trend. It is apparent that the BL Lacs have a higher mean γ-ray loudness value because many of them have synchrotron peaks above ∼ 10^{15} Hz. Since the fixed radio bandpass is always located below the synchrotron peak, if we compare two BL Lacs with identical SED shapes but different synchrotron peak locations, the high synchrotron peaked BL Lac will have a lower radio flux density, and thus a higher γ-ray loudness value. Figure 6 shows this broad trend for the BL Lacs, with the HSP jets having generally lower radio flux densities than the LSPs.

A similar spectral index effect also occurs as the high energy SED peak moves in tandem through the *Fermi* LAT band as the synchrotron peak frequency increases. This is manifested in the strong correlation seen between the γ-ray photon spectral index α_G and synchrotron peak frequency for the 1FGL blazars, as described by Abdo et al. (2010d). In Figure 7 we plot γ-ray loudness against photon spectral index. Again we see a good (even tighter) linear correlation for the BL Lac objects, and no trend for the quasars. A regression fit to the BL Lacs, omitting the outlier source J0825+0309, gives $\log G_r = (-2.3 \pm 0.2) \alpha_G + 7.8 \pm 0.5$, with a scatter of 0.3 dex.

The continuous trend from LSP to HSP BL Lacs in Figures 5 and 7 is noteworthy, since it implies a relatively narrow intrinsic range of variation in the SED shapes of the brightest BL Lac objects. Broadly speaking, there are three aspects of a SED that can affect its measured γ-ray loudness parameter. These are the relative positions of the synchrotron and high energy peaks with respect to the fixed γ-ray and radio bands, their relative luminosities (often referred to as the Compton dominance), and the width and shape of each peak. If we take the simplest case of both peaks having equal luminosity and identical parabolic forms in $\nu F_\nu - \nu$ space, then we would expect to have

$$\log G_r = C_1 \left(\log \frac{\nu_h}{\nu_\gamma} \right)^2 - C_2 \left(\log \frac{\nu_s}{\nu_r} \right)^2, \qquad (5)$$

where ν_γ and ν_r are the frequencies of the LAT γ-ray and VLBA radio bands, ν_h and ν_s are the frequencies of the high energy and synchrotron peaks, and C_1 and C_2 are parameters
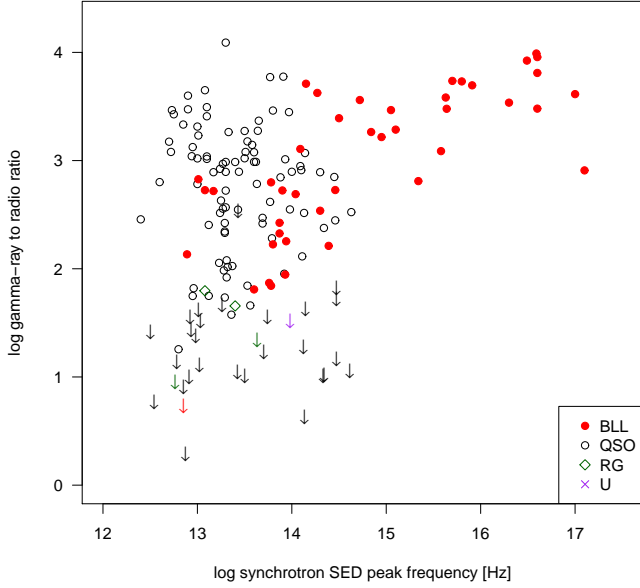
Figure 5. γ-ray to radio luminosity ratio G_r versus synchrotron SED peak frequency. The red filled circles represent BL Lac objects, the open circles quasars, the green diamonds radio galaxies, and the purple crosses optically unidentified objects. The arrows denote upper-limits. The BL Lac objects show a linear trend of increasing γ-ray loudness with SED peak frequency, while no trend exists for the quasars.
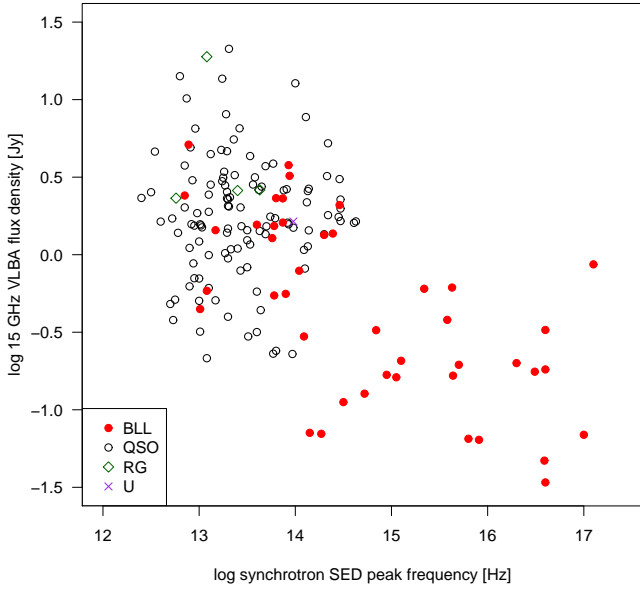
Figure 6. 15 GHz VLBA flux density versus synchrotron SED peak frequency. The red filled circles represent BL Lac objects, the open circles quasars, the green diamonds radio galaxies, and the purple crosses optically unidentified objects.

that determine their respective widths.

If both SED peaks have identical parabolic shape ($C_1 = C_2$) and the entire SED is then shifted to a higher frequency, such that the peak separation $\log \nu_h - \log \nu_s = C_3$ remains constant, then we would expect to find a linear relation of the form $\log G_r = a \log \nu_s$, with slope

$$a = 2C_1 \left(\log \frac{\nu_r}{\nu_\gamma} + C_3 \right). \qquad (6)$$
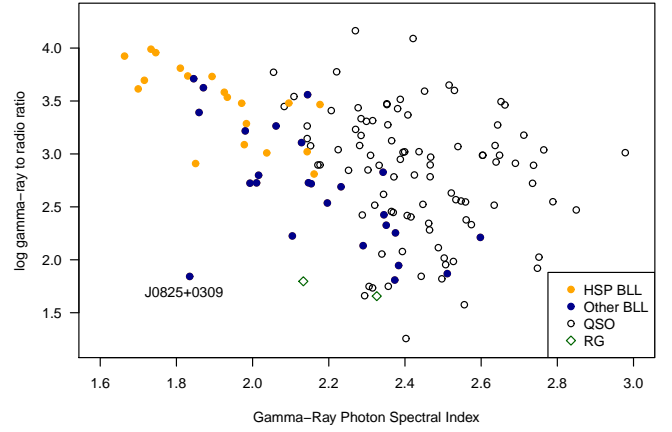
Figure 7. Plot of γ-ray to radio luminosity ratio G_r versus γ-ray photon spectral index. The filled circles represent BL Lac objects, with the high synchrotron peaked ones in orange and others in blue. The open circles represent quasars, and the green diamonds radio galaxies. The BL Lac objects show a log-linear trend of decreasing γ-ray loudness with photon spectral index, while no trend exists for quasars.

From compilations of observed blazar SEDs (e.g., Abdo et al. 2010e; Chang 2010) we know that in actuality, SED peak shapes are only approximately parabolic, and that there exists a range of C parameter values among the population. These factors would tend to distort any trend between $\log \nu_s$ and $\log G_r$ from the simple linear one described here. Furthermore, an intrinsic range of Compton dominance parameter would likely destroy any linear relation completely. The fact that we see a scatter of only 0.5 dex for the BL Lac objects therefore implies that the SEDs of the brightest AGNs of this class must have relatively similar shapes, at least much more so than the quasars, which show no ν_s-G_r correlation. Our results are corroborated by a recent study of the 1LAC by Gupta et al. (2011), who defined a "Compton efficiency" parameter as the ratio of the high-energy (inverse Compton) SED peak luminosity to 8 GHz radio VLA core luminosity. They found a similar trend of higher Compton efficiency with increasing synchrotron peak frequency for BL Lac objects, but no trend for FSRQs.

So far in this discussion we have omitted the possible effects of relativistic beaming on the SED. For the simple case of the same Doppler factor in both the radio and γ-ray-emitting regions, the entire SED should be blue-shifted by the Doppler factor, and the apparent luminosity of both peaks will be increased by Doppler boosting. Models which attribute the high energy peak to inverse Compton scattering of external seed photons by relativistic electrons in the jet predict a higher Doppler boost in γ-rays, because of the additional Lorentz transformation between the seed photon and jet rest frames (Dermer 1995). In this case, when considering a jet at smaller viewing angle, the resulting increase in Doppler factor boosts the luminosity of the high energy peak to a level much higher than the synchrotron peak, thereby increasing the observed Compton dominance and γ-ray loudness. If the seed photons are internal to the jet, for a single-zone synchrotron self-Compton (SSC) model relatively equal boosting is expected in both regimes; thus G_r in this case is much less sensitive to Doppler boosting. The fairly good linear G_r-ν_s correlation for the BL Lacs therefore favors the SSC process as the dominant emission mechanism in this class of blazars. This is in general agreement with the conclusions of recent studies
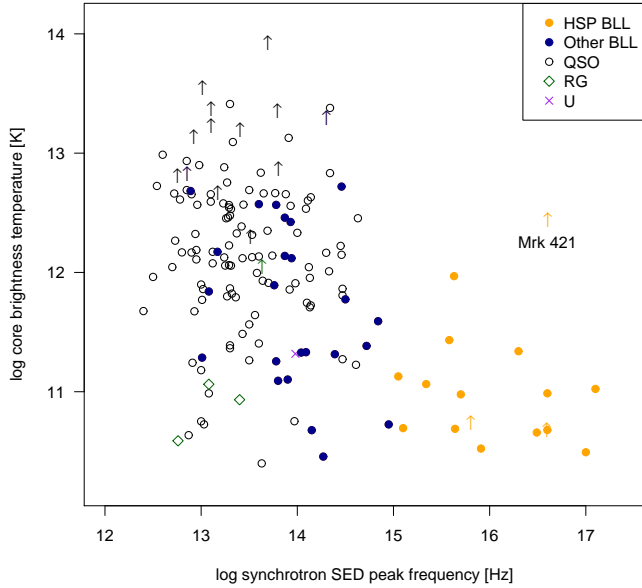
Figure 8. Radio core brightness temperature at 15 GHz versus synchrotron SED peak frequency. The filled circles represent BL Lac objects, with the high synchrotron peaked ones in orange and others in blue. The open circles represent quasars, the green diamonds radio galaxies, and the purple crosses optically unidentified objects. The arrows denote lower limits. The radio cores of the high-synchrotron SED peak BL Lac objects tend to be less compact than the other AGNs in our sample. J1104+3812 (Mrk 421) is the only high-synchrotron peaked blazar in the sample with a high core brightness temperature. Not plotted is the unusually low-brightness temperature quasar J0957+5522 (4C +55.17) at $\nu_s = 10^{13.77}$ Hz, $T_b = 10^{8.46}$ K.

which have modeled the SEDs of *Fermi*-detected blazars with detailed synchrotron and inverse-Compton emission models (Abdo et al. 2010e). It should be possible to investigate this issue in much greater depth when more detailed information on the SED parameters of our full sample can be obtained.

4.3. *Parsec-Scale Radio Jet Properties*
4.3.1. *Core Brightness Temperature*

Nearly all of the AGNs in our sample have a parsec-scale radio jet morphology that is dominated by a bright, flat-spectrum core, which is often unresolved or barely resolved in our mas-scale VLBA images. At our observing frequency of 15 GHz, this core typically represents the region where the jet becomes optically thick, with the true jet nozzle being located upstream (Sokolovsky et al. 2011). The brightness temperature of the core component in our VLBA images measures the compactness of the radio jet emission, and has been previously shown to be correlated with indicators of relativistic beaming, such as superluminal apparent speed (Homan et al. 2006) and radio flux density variability (Tingay et al. 2001; Hovatta et al. 2009).

In Figure 8 we plot core brightness temperature against synchrotron SED peak frequency. The main visible trend is that the HSP BL Lac radio cores tend to be less compact than those of the other AGNs in the sample. We discuss the possible ramifications of this trend on beaming and jet velocity stratification models for HSP BL Lacs in § 4.4.

4.3.2. *Apparent Jet Opening Angles*

In a previous study of the MOJAVE sample using the initial 3 months of *Fermi* data, Pushkarev et al. (2009) found a tendency for the γ-ray-detected blazars to have wider apparent
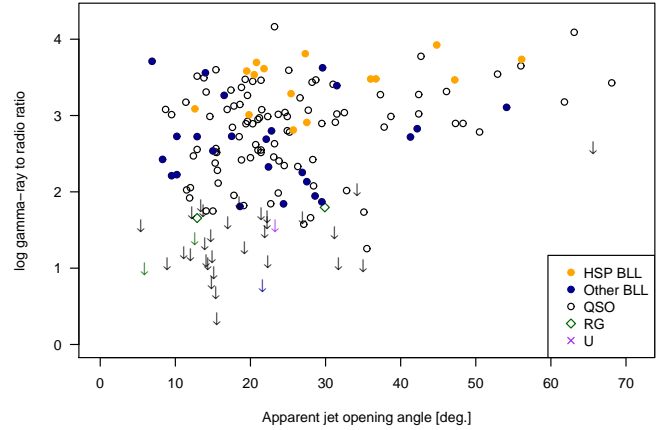
Figure 9. γ-ray to radio luminosity ratio versus apparent jet opening angle. The filled circles represent BL Lac objects, with the high synchrotron peaked ones in orange and others in blue. The open circles represent quasars, the green diamonds radio galaxies, and the purple crosses optically unidentified objects. The AGNs with wide apparent opening angles tend to have high γ-ray loudness values.

opening angles than the non-detected ones. Since the calculated intrinsic opening angles of the two groups were similar, they concluded that the γ-ray-detected jets were viewed more closely to the line of sight.

We have analyzed the apparent jet opening angles of our sample, and find that they range from 5 to 68 degrees, with a mean of 24 degrees. There is an extended tail to the distribution, with 19 jets having opening angles greater than 40 degrees. With the exception of the quasar J0654+4514, none of the high opening angle jets are highly variable (radio modulation indices all less than 0.26). We find no statistically discernible differences in the opening angle distributions of the different optical or SED classes. We do find a correlation between γ-ray loudness and apparent opening angle, however the relationship is non-linear (Fig. 9). All of the AGNs in the high-opening angle tail (> 40 deg.) of the distribution are significantly γ-ray-loud ($G_r > 100$). The apparent opening angle of a jet is related to the viewing angle and intrinsic opening angle, with smaller intrinsic angles expected for high Lorentz factor jets based on hydrodynamical considerations (Jorstad et al. 2005). The high opening angle jets in our sample are a mixture of BL Lac objects and FSRQ, with a range of synchrotron SED peak frequencies. With jet kinematic information on the sample from the MOJAVE program it will be possible to investigate whether these particular jets are viewed unusually close to the line of sight, or have atypically large intrinsic opening angles.

4.3.3. *Radio Core Polarization Vectors*

We compared the direction of the linear polarization vector at the radio core position to the mean jet position angle for our sources, as described in § 3.2. In some sources such as PKS 1502+106 (Abdo et al. 2010b) and PMN J0948+0022 (Foschini et al. 2011), changes in the core polarization angle have been seen to occur in conjunction with γ-ray flaring events, suggesting a close connection between the radio and γ-ray emission regions. We do not find any correlations between the core polarization vector offset and any γ-ray or SED properties for our sample. However, since the linear polarization vector angles tend to be highly variable in blazars (Jorstad et al. 2005), a more detailed analysis would require
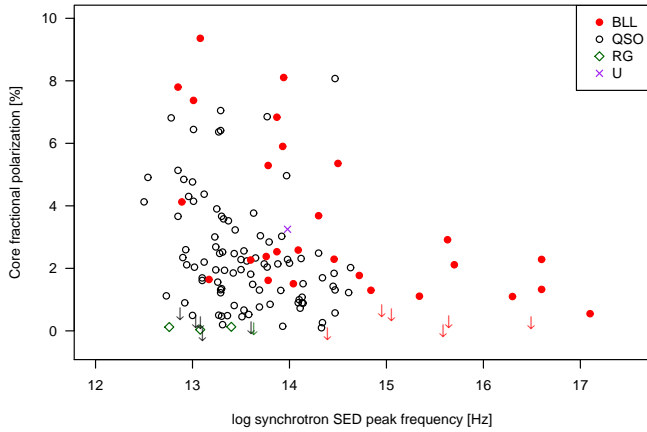
Figure 10. Linear fractional polarization level of VLBA radio core at 15 GHz versus synchrotron SED peak frequency. The red filled circles represent BL Lac objects, the open circles quasars, the green diamonds radio galaxies, and the purple crosses optically unidentified objects. The arrows denote upper-limits.

truly simultaneous VLBA-*Fermi* measurements rather than the average γ-ray data that we use in our current study. Another possible reason for the lack of correlations is Faraday effects in the cores, which can rotate the observed polarization vectors. We are currently completing a VLBA rotation measure analysis of the original MOJAVE radio-selected sample (Hovatta et al. 2011) to further investigate this effect.

4.3.4. *Radio Core Polarization Level*

In Figure 10 we plot the linear fractional polarization level of the VLBA core at the reference epoch versus SED peak frequency. In general the cores of the jets are weakly polarized (< 4 %), with increasing fractional polarization levels seen downstream (Lister & Homan 2005). There are no appreciable differences in the BL Lac and FSRQ core polarization distributions, however, as we discuss in section 4.4, the high synchrotron peak BL Lacs tend to have low core polarization levels. We find no trend between 15 GHz radio core polarization and γ-ray loudness, although in the VIPS 5 GHz VLBA survey (Linford et al. 2011) detected core polarization more frequently in LAT-detected AGNs than in the non-LAT ones. We note that the core polarizations tend to vary over time in these jets, which can complicate such analyses. Indeed, in a preliminary investigation of the original MOJAVE radio flux-limited sample, we found the LAT-detected AGNs tended to have higher median fractional core polarization levels during the first three months of the Fermi mission, as compared to their historical average level (Hovatta et al. 2010). A more complete polarization analysis of our full multi-epoch MOJAVE VLBA dataset will be presented in a forthcoming study.

4.3.5. *Radio Variability*

The hallmark flux variability seen in blazars is believed to be closely related to Doppler beaming (Aller et al. 1992; Lähteenmäki et al. 1999; Hovatta et al. 2009) since it can significantly heighten the magnitudes of flaring events and shorten their apparent timescales (e.g., Lister 2001b). AGN jets have also been found to be in a more active radio state within several months from LAT-detection of their strong γ-ray emission (Kovalev et al. 2009; Pushkarev et al. 2010). The AGNs in our sample are indeed highly variable, with 51
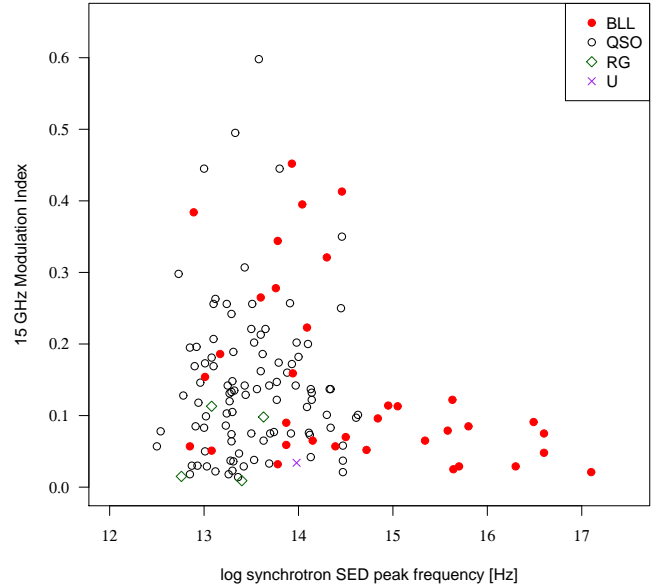
Figure 11. Radio modulation index at 15 GHz versus synchrotron SED peak frequency. The filled circles represent BL Lac objects, the open circles quasars, the plus symbols radio galaxies, and the crosses optically unidentified objects. None of the blazars with synchrotron SED peaks above 10^{15} Hz show high amplitude radio variability.

of 144 sources having standard deviations greater than 15% of their mean flux density level over an 11 month period. In their full sample of over 1000 sources, Richards et al. (2011) found the FSRQs to have significantly higher variability amplitudes than the BL Lacs. We do not see this distinction in our sample, however, most likely because ours contains a smaller proportion of high-synchrotron peaked BL Lacs. The latter tend to have moderately low radio modulation indexes, as seen in Figure 11.

4.4. *High Synchrotron Peaked AGN Jets and the BL Lac Blazar Class*

Previous studies of the full 1LAC catalog by the LAT team (Abdo et al. 2010d,e) have established that HSP BL Lacs have fundamentally different γ-ray properties than the γ-ray-loud FSRQs. In our study we have found that the HSP BL Lacs are characterized by high γ-ray to radio luminosity ratios and lower than average radio core compactness. Given these differences seen in both the radio and γ-ray regimes, a fundamental question remains as to whether the lower synchrotron-peaked BL Lacs also form a jet population distinct from the FSRQs. The continuity of the trend between SED peak frequency and γ-ray loudness (Figure 5) would suggest that their SED shapes are similar to the HSP BL Lacs, and thus they should be unified with them. They are also more similar to the HSPs in terms of their radio luminosity, as compared to the generally more luminous FSRQs (Figure 3).

If we directly compare the radio properties of the LSP BL Lacs and LSP FRSQs in our sample, we find that the LSP BL Lacs have higher mean fractional linear polarization (4.8 ± 2.8 versus 2.5 ± 1.7; t=3.02, p=0.992 according to a Welch Two Sample t-test), although both classes span roughly the same range of extreme values (Fig. 10). It is possible that beam depolarization effects may lower the mean value for the FSRQs, since they are typically at higher redshift than the BL Lacs and are thus imaged with poorer spatial resolution.

However, if we compare the LSP and HSP BL Lacs, which have similar redshift ranges, we find the latter have consistently low core polarization and modulation indices, as well as lower than average radio core brightness temperatures. Since high radio variability, core polarization, and brightness temperature are generally associated with high Doppler boosted-jets (e.g., Lister 2001a; Tingay et al. 2001; Hovatta et al. 2009), the trends we find in our sample support the following scenario for the brightest γ-ray and radio blazars in the sky. Because of their higher intrinsic γ-ray loudness ratios and low redshifts, the HSP BL Lacs do not need to be as highly beamed to enter into flux-limited γ-ray and radio samples, thus they tend to have lower Doppler boosting factors than other blazar classes. The LSP BL Lacs are less intrinsically luminous than the FSRQs, but their moderately high intrinsic γ-ray loudness ratios and Doppler boosting factors combine to give them apparent γ-ray and radio luminosities comparable to the fainter end of the FSRQ distribution.

The above scenario is supported by the previous results of Nieppola et al. (2008), who found a general trend of decreasing Doppler factor with increasing synchrotron SED peak frequency. Their sample only included blazars of the LSP and ISP class, however. A potential test can be made with parsec-scale superluminal motion measurements, which set an upper limit on the viewing angle and a lower limit on the bulk jet Lorentz factor (see e.g., Urry & Padovani 1995). One of the main unresolved problems for HSP BL Lacs has been the relatively slow apparent jet speeds detected for these objects (Piner & Edwards 2004; Piner et al. 2010), despite the need for large Doppler factors to account for rapid variability seen in γ-rays and to accurately model their SEDs (see, e.g., Henri & Saugé 2006). Several models have been put forward to address this "Doppler factor crisis", including decelerating flows (Georganopoulos & Kazanas 2003), and stratified spine-sheath models (Celotti et al. 2001; Tavecchio & Ghisellini 2008), in which the γ-rays originate in a high-velocity jet spine, while the radio emission (and moving blobs) are associated with a lower-Lorentz factor sheath. In this manner the radio and γ-ray emission can have independent Doppler factors. As we discussed in § 3.3, however, uncorrelated beaming factors for the synchrotron and high-energy peaks would likely destroy any linear relation between SED synchrotron peak and γ-ray loudness, in contrast to what we see for the BL Lacs in our survey (Figure 5). A more recent model put forward by Lyutikov & Lister (2010) involving non-steady magnetized outflows suggests the existence of different, yet correlated Doppler factors for the two SED peak regions, which can potentially preserve the G_r versus synchrotron SED peak relation. With the MOJAVE program we are currently obtaining multi-epoch VLBA measurements of all the γ-ray-selected radio jets in our sample, which will allow us to further investigate the connections between synchrotron SED peak frequency, apparent jet speed, jet opening angle, and Doppler factor in the brightest blazars.

5. SUMMARY

We have obtained single-epoch 15 GHz MOJAVE program VLBA images[68] of two complete flux-limited samples of blazars north of declination −30° and > 10° from the Galactic plane. The first sample consists of the brightest sources associated with AGNs that were detected by the *Fermi* LAT instrument during its first 11 months of operations. The second

[68] MOJAVE data archive: http://www.physics.purdue.edu/MOJAVE

sample contains all radio-loud AGNs known to have exceeded a 15 GHz VLBA flux density of 1.5 Jy during the same time period. There are 116 AGNs in the γ-ray-selected sample and 105 AGNs in the matching radio one, with 48 AGNs in common to both samples. By covering two complete regions of the γ-ray-radio flux plane, we are able to sample the widest possible range of γ-ray loudness in bright blazars. Our results can be compared with those of Linford et al. (2011), who studied a larger, radio flux-limited sample of fainter AGNs with 5 GHz VLBA data obtained several years before the launch of *Fermi* . We summarize our major findings as follows:

1. There is a 28% overlap in our samples of the brightest γ-ray-and radio-selected AGNs in the northern sky. We find no major differences in the sample redshift distributions, with the exception of a small number of high-synchrotron peaked (HSP) BL Lac objects which appear only in the γ-ray-selected sample. At the highest flux levels therefore, γ-ray-and radio-selected blazars are essentially selected from the same general parent population.

2. We have tabulated a γ-ray loudness parameter (G_r) for all of the sources in our sample, including upper limits for the non-LAT associated sources in our radio-selected sample. The non-censored G_r values span nearly four orders of magnitude, reflecting the wide range of SED parameters in the bright blazar population. However, within the BL Lac optical class, we find a linear relation (scatter = 0.5 dex) between synchrotron SED peak frequency ν_s and G_r, with the HSP BL Lacs being more γ-ray-loud. Such a linear relationship is expected if the overall range of SED shape is relatively narrow within the BL Lac population, as the radio flux density will drop and γ-ray flux will increase as the SED is successively shifted to higher frequencies, thereby increasing the γ-ray loudness. A further consequence of the observed correlation is that the amount of Doppler boosting must be correlated in the radio and γ-ray emission regimes of BL Lac jets. The external seed-photon inverse-Compton model is not favored for the γ-ray emission of the BL Lacs in our sample, since it predicts higher boosting of the γ-rays with respect to the radio. Any range of Doppler factor within the BL Lac population would therefore destroy any expected linear correlation between G_r and ν_s in the external Compton scenario.

3. In terms of their 15 GHz radio properties, the HSP BL Lac objects in our sample are distinguished by their lower than average radio core brightness temperatures. None of them display large radio modulation indices or high linear core polarization levels. Given the known association of such properties with relativistic beaming, we suggest that the HSP BL Lacs have generally lower Doppler factors than the lower-synchrotron peaked BL Lacs or FSRQs in our sample. They are able to meet our flux-selection criteria primarily because of their high intrinsic γ-ray ratios and low redshifts. The continuity of the observed G_r - ν_s relation suggests that the high- and low-synchrotron peaked BL Lacs are part of the same parent population. The latter have moderate intrinsic γ-ray loudness ratios and Doppler boosting factors which combine to give them apparent γ-ray and radio luminosities that are comparable to the fainter end of the FSRQ distribution.

4. We confirm the results of a previous analysis by Pushkarev et al. (2009), who found that *Fermi* -associated AGNs tend to have wider apparent jet opening angles. Using a larger (11 month versus 3 month) *Fermi* dataset on our more comprehensive blazar sample, we find that all of the highest opening angle jets (> 40°) in our sample are significantly γ-

ray loud.

The MOJAVE program is continuing to investigate these issues by obtaining multi-epoch VLBA measurements of all the γ-ray-selected radio jets in our sample. Together with more complete SED information, light curves and deep EVLA images we aim to gain a fuller understanding of the connections between synchrotron SED peak frequency, Compton dominance, apparent jet speed, and Doppler factor in the brightest blazars.

APPENDIX

REDSHIFT INFORMATION

We summarize the current status of those blazars in our sample which either do not have a spectroscopic redshift listed in Table 1, or have uncertain or conflicting reported redshift values in the literature.

J0050–0929: — The NED value of $z = 0.634$ from Rector & Stocke (2001) is based on a very weak emission line and is listed by those authors as tentative. This line was not seen by Shaw et al. (2009) or Sbarufatti et al. (2006) in their optical spectra. Based on the absence of host galaxy absorption features in the optical spectrum Shaw et al. (2009) find $z > 0.44$, and Sbarufatti et al. (2006) find $z > 0.3$. Meisner & Romani (2010) obtain $z > 0.27$ based on the measured optical host galaxy magnitude.

J0112+2244: — Healey et al. (2008) list $z = 0.265$ based on an unpublished spectrum. Shaw et al. (2009) find $z > 0.24$ and Sbarufatti et al. (2009) get $z > 0.25$ based on the absence of host galaxy absorption features in the optical spectrum.

J0120–2701: — The NED value of $z = 0.559$ is a lower limit from Stickel et al. (1993a).

J0136+3908: — We could not find any published redshift value for this source.

J0237+2848: — The NED value of $z = 1.213$ attributed to Schmidt (1977) is different than the $z = 1.207$ that is reported in that reference.

J0222+4302 = 3C 66A: — As discussed by Finke et al. (2008) and Bramel et al. (2005), the NED redshift value of $z = 0.444$ is highly unreliable. Finke et al. (2008) obtained $z > 0.096$ based on their optical spectrum.

J0316+0904: — We could not find any published redshift value for this source.

J0433+2905: — Meisner & Romani (2010) obtain $z > 0.48$ based on the measured optical host galaxy magnitude. The origin of the $z = 0.97$ value listed in BZCAT (Massaro et al. 2009) is unknown.

J0509+0541: — Meisner & Romani (2010) obtain $z > 0.38$ based on the measured optical host galaxy magnitude.

J0608–1520: — Shaw et al. (2011) have obtained an optical spectrum of this source and find emission lines indicating a quasar at $z = 1.094$.

J0612+4122: — Meisner & Romani (2010) obtain $z > 0.69$ based on the measured optical host galaxy magnitude.

J0630-2406: — Landt & Bignall (2008) list $z = 1.238$, which is a lower limit based on Mg II absorption lines in their unpublished optical spectrum.

J0654+5042: — Shaw et al. (2011) have obtained an optical spectrum of this source and find emission lines indicating a quasar at $z = 1.253$.

J0738+1742: — The NED value of $z = 0.424$ is a lower limit determined by Rector & Stocke (2001) on the basis of absorption systems in the optical spectrum.

J0818+4222: — Britzen et al. (2008) list $z = 0.245$ based on an unpublished spectrum. The NED value of $z = 0.53$ is attributed to Sowards-Emmerd et al. (2005) but does not appear in that paper. An optical spectrum obtained by Shaw et al. (2011) shows no visible features. Sbarufatti et al. (2005) found $z > 0.75$ based on a lower limit to the host galaxy magnitude.

J1037+5711: — Véron-Cetty & Véron (2000) classify this source as a BL Lac object. We were unable to find any redshift value in the literature.

J1248+5820: — The SDSS optical spectrum (Abazajian et al. 2005) yields no reliable redshift, and an unpublished spectrum by Shaw et al. (2011) shows no spectral features.

J1215−1731: — We were not able to find any published redshift value for this optically unidentified source, which lies extremely close on the sky to a bright star.

J1221+2813 = W Comae: — The NED redshift value of $z = 0.102$ is likely incorrect, as discussed by Finke et al. (2008). The latter authors constrain the redshift to $z > 0.104$ using their optical spectrum.

J1303+2433: — Glikman et al. (2007) list $z = 0.993$ but give no reference for the origin of this redshift. An optical spectrum obtained by Shaw et al. (2011) yields $z > 0.769$.

J1427+2348: — Shaw et al. (2009) find $z > 0.03$, while Meisner & Romani (2010) get $z > 0.23$ based on host galaxy magnitude.

J1516+1932: — The NED redshift value of $z = 1.07$ from Persic & Salucci (1986) is based on tentative identifications of very faint emission lines in the optical spectrum of Wilkes et al. (1983), and has not been subsequently confirmed. An optical spectrum obtained by Shaw et al. (2011) shows no spectral features.

J1532+6129: — Shaw et al. (2009) find $z > 0.63$ based on the absence of host galaxy absorption features in the optical spectrum, while Meisner & Romani (2010) obtain $z > 0.39$ based on the measured optical host galaxy magnitude.

J1555+1111: — The $z = 0.360$ redshift value from Miller & Green (1983) was shown by Falomo & Treves (1990) and Falomo et al. (1994) to be incorrect. Based on the absence of host galaxy absorption features in the optical spectrum, Sbarufatti et al. (2006) find $z > 0.09$. Danforth et al. (2010) analyze the Lyman absorber properties of the far-UV spectrum of this source and find $0.395 < z < 0.58$.

J1719+1745: — Sowards-Emmerd et al. (2005) list $z = 0.137$ based on an unpublished optical spectrum. Shaw et al. (2009) obtain $z > 0.58$ based on the measured optical host galaxy magnitude.

J1725+1152: — As described by Sbarufatti et al. (2006), the tentative NED redshift of $z = 0.018$ from Griffiths et al. (1989) has not been confirmed in several subsequent spectroscopic observations. Based on the absence of host galaxy absorption features in the optical spectrum, Sbarufatti et al. (2006) find $z > 0.17$.

J1903+5540: — Meisner & Romani (2010) obtain $z > 0.58$ based on the measured optical host galaxy magnitude.

J2236−1433: — Sbarufatti et al. (2006) trace the oft-cited erroneous NED redshift of $z = 0.325$ to a clerical error. Based on the absence of host galaxy absorption features in the optical spectrum, they find find $z > 0.65$. An unpublished optical spectrum by Shaw et al. (2011) shows no spectral features.

J2243+2021: — Meisner & Romani (2010) obtain $z > 0.39$ based on the measured optical host galaxy magnitude.

REFERENCES

Aatrokoski, J., e. a. 2011, ArXiv e-prints,1101.2047
Abazajian, K., et al. 2004, AJ, 128, 502
—. 2005, AJ, 129, 1755
Abdo, A. A., et al. 2009, ApJ, 700, 597
—. 2010a, ApJS, 188, 405
—. 2010b, ApJ, 710, 810
—. 2010c, ApJ, 710, 1271
—. 2010d, ApJ, 715, 429
—. 2010e, ApJ, 716, 30
Abdo et al., A. 2011, ArXiv e-prints, 1108.1435
Adelman-McCarthy, J. K., et al. 2008, ApJS, 175, 297
Akiyama, M., Ueda, Y., Ohta, K., Takahashi, T., & Yamada, T. 2003, ApJS, 148, 275
Albert, J., et al. 2007, ApJ, 667, L21
Aller, M. F., Aller, H. D., & Hughes, P. A. 1992, ApJ, 399, 16
—. 2003, ApJ, 586, 33
Arshakian, T. G., Leon-Tavares, J., Böttcher, M., Torrealba, J. M., Chavushyan, V. H., Lister, M. L., Ros, E., & Zensus, J. 2011, in prep.
Baker, J. C., Hunstead, R. W., Kapahi, V. K., & Subrahmanya, C. R. 1999, ApJS, 122, 29
Boisse, P., & Bergeron, J. 1988, A&A, 192, 1
Bramel, D. A., et al. 2005, ApJ, 629, 108
Britzen, S., et al. 2008, A&A, 484, 119
Browne, I. W. A., Savage, A., & Bolton, J. G. 1975, MNRAS, 173, 87P
Burbidge, E. M. 1970, ApJ, 160, L33
Celotti, A., Ghisellini, G., & Chiaberge, M. 2001, MNRAS, 321, L1
Chang, C. 2010, PhD thesis, Max-Planck-Institut für Radioastronomie
Cognard, I., et al. 2011, ArXiv e-prints,1102.4192
Cohen, R. D., Smith, H. E., Junkkarinen, V. T., & Burbidge, E. M. 1987, ApJ, 318, 577
Condon, J. J., Cotton, W. D., Greisen, E. W., Yin, Q. F., Perley, R. A., Taylor, G. B., & Broderick, J. J. 1998, AJ, 115, 1693
Danforth, C. W., Keeney, B. A., Stocke, J. T., Shull, J. M., & Yao, Y. 2010, ApJ, 720, 976
de Grijp, M. H. K., Keel, W. C., Miley, G. K., Goudfrooij, P., & Lub, J. 1992, A&AS, 96, 389
Deller, A. T., et al. 2011, PASP, 123, 275
Dermer, C. D. 1995, ApJ, 446, L63
di Serego-Alighieri, S., Danziger, I. J., Morganti, R., & Tadhunter, C. N. 1994, MNRAS, 269, 998
Dondi, L., & Ghisellini, G. 1995, MNRAS, 273, 583
Drinkwater, M. J., et al. 1997, MNRAS, 284, 85
Ellison, S. L., Yan, L., Hook, I. M., Pettini, M., Wall, J. V., & Shaver, P. 2001, A&A, 379, 393
Falomo, R., Scarpa, R., & Bersanelli, M. 1994, ApJS, 93, 125
Falomo, R., & Treves, A. 1990, PASP, 102, 1120
Falomo, R., & Ulrich, M.-H. 2000, A&A, 357, 91
Finke, J. D., Shields, J. C., Böttcher, M., & Basu, S. 2008, A&A, 477, 513
Foschini, L. 2011, in Proceedings of the conference "Narrow-Line Seyfert 1 Galaxies and their place in the Universe". April 4-6, 2011. Milano, Italy. Editorial Board: Luigi Foschini (chair), Monica Colpi, Luigi Gallo, Dirk Grupe, Stefanie Komossa, Karen Leighly, Smita Mathur. Published online at <A href="http://pos.sissa.it/cgi-bin/reader/conf.cgi?confid=126">http://pos.sissa.it/cgi-bin/reader/conf.cgi?confid=126</A>, id.24
Foschini, L., et al. 2011, MNRAS, 413, 1671
Fricke, K. J., Kollatschny, W., & Witzel, A. 1983, A&A, 117, 60
Georganopoulos, M., & Kazanas, D. 2003, ApJ, 594, L27
Glikman, E., Helfand, D. J., White, R. L., Becker, R. H., Gregg, M. D., & Lacy, M. 2007, ApJ, 667, 673
Griffiths, R. E., Wilson, A. S., Ward, M. J., Tapia, S., & Ulvestad, J. S. 1989, MNRAS, 240, 33
Gupta, J. A., Browne, I. W. A., & Peel, M. W. 2011, ArXiv e-prints, 1106.5172
Halpern, J. P., Eracleous, M., & Mattox, J. R. 2003, AJ, 125, 572
Hartman, R. C., et al. 1999, ApJS, 123, 79
Healey, S. E., et al. 2008, ApJS, 175, 97
Helene, O. 1983, Nuclear Instruments and Methods in Physics Research, 212, 319
Henri, G., & Saugé, L. 2006, ApJ, 640, 185
Henstock, D. R., Browne, I. W. A., Wilkinson, P. N., & McMahon, R. G. 1997, MNRAS, 290, 380

Hewett, P. C., Foltz, C. B., & Chaffee, F. H. 1995, AJ, 109, 1498
Hewitt, A., & Burbidge, G. 1991, ApJS, 75, 297
Ho, L. C., & Kim, M. 2009, ApJS, 184, 398
Homan, D. C., et al. 2006, ApJ, 642, L115
Hovatta, T., Lister, M. L., Aller, M. F., Aller, H. D., Homan, D. C., Kovalev, Y. Y., Pushkarev, A. B., & Savolainen, T. 2011, ArXiv e-prints,1108.1514
Hovatta, T., Lister, M. L., Kovalev, Y. Y., Pushkarev, A. B., & Savolainen, T. 2010, International Journal of Modern Physics D, 19, 943
Hovatta, T., Valtaoja, E., Tornikoski, M., & Lähteenmäki, A. 2009, A&A, 498, 723
Hunter, S. D., et al. 1993, ApJ, 409, 134
Impey, C. D., & Neugebauer, G. 1988, AJ, 95, 307
Jackson, N., & Browne, I. W. A. 1991, MNRAS, 250, 414
Jones, D. H., et al. 2009, MNRAS, 399, 683
Jorstad, S. G., Marscher, A. P., Mattox, J. R., Wehrle, A. E., Bloom, S. D., & Yurchenko, A. V. 2001, ApJS, 134, 181
Jorstad, S. G., et al. 2005, AJ, 130, 1418
Junkkarinen, V. 1984, PASP, 96, 539
Kellermann, K. I., Vermeulen, R. C., Zensus, J. A., & Cohen, M. H. 1998, AJ, 115, 1295
Kellermann, K. I., et al. 2004, ApJ, 609, 539
Komatsu, E., et al. 2009, ApJS, 180, 330
Kovalev, Y. Y. 2009, ApJ, 707, L56
Kovalev, Y. Y., et al. 2005, AJ, 130, 2473
—. 2009, ApJ, 696, L17
Lähteenmäki, A., Valtaoja, E., & Wiik, K. 1999, ApJ, 511, 112
Landt, H., & Bignall, H. E. 2008, MNRAS, 391, 967
Landt, H., Padovani, P., & Giommi, P. 2002, MNRAS, 336, 945
Lawrence, C. R., Zucker, J. R., Readhead, A. C. S., Unwin, S. C., Pearson, T. J., & Xu, W. 1996, ApJS, 107, 541
Linford, J. D., et al. 2011, ApJ, 726, 16
Lister, M. L. 2001a, ApJ, 562, 208
—. 2001b, ApJ, 561, 676
Lister, M. L., & Homan, D. C. 2005, AJ, 130, 1389
Lister, M. L., Homan, D. C., Kadler, M., Kellermann, K. I., Kovalev, Y. Y., Ros, E., Savolainen, T., & Zensus, J. A. 2009a, ApJ, 696, L22
Lister, M. L., et al. 2009b, AJ, 137, 3718
—. 2009c, AJ, 138, 1874
Lynds, C. R. 1967, ApJ, 147, 837
Lyutikov, M., & Lister, M. 2010, ApJ, 722, 197
Marziani, P., Sulentic, J. W., Dultzin-Hacyan, D., Calvani, M., & Moles, M. 1996, ApJS, 104, 37
Massaro, E., Giommi, P., Leto, C., Marchegiani, P., Maselli, A., Perri, M., Piranomonte, S., & Sclavi, S. 2009, A&A, 495, 691
Mattox, J. R., et al. 1996, ApJ, 461, 396
McConville, W., et al. 2011, ArXiv e-prints,1107.1471
McIntosh, D. H., Rieke, M. J., Rix, H.-W., Foltz, C. B., & Weymann, R. J. 1999, ApJ, 514, 40
Meisner, A. M., & Romani, R. W. 2010, ApJ, 712, 14
Michel, A., & Huchra, J. 1988, PASP, 100, 1423
Miller, H. R., & Green, R. F. 1983, in Bulletin of the American Astronomical Society, 957
Nieppola, E., Tornikoski, M., & Valtaoja, E. 2006, A&A, 445, 441
Nieppola, E., Valtaoja, E., Tornikoski, M., Hovatta, T., & Kotiranta, M. 2008, A&A, 488, 867
Nilsson, K., Pursimo, T., Sillanpää, A., Takalo, L. O., & Lindfors, E. 2008, A&A, 487, L29
Osmer, P. S., Porter, A. C., & Green, R. F. 1994, ApJ, 436, 678
Persic, M., & Salucci, P. 1986, in Astrophysics and Space Science Library, Vol. 121, Structure and Evolution of Active Galactic Nuclei, ed. G. Giuricin, M. Mezzetti, M. Ramella, & F. Mardirossian, 675–677
Peterson, B. A., Wright, A. E., Jauncey, D. L., & Condon, J. J. 1979, ApJ, 232, 400
Piner, B. G., & Edwards, P. G. 2004, ApJ, 600, 115
Piner, B. G., Pant, N., & Edwards, P. G. 2010, ApJ, 723, 1150
Pushkarev, A. B., Kovalev, Y. Y., & Lister, M. L. 2010, ApJ, 722, L7
Pushkarev, A. B., Kovalev, Y. Y., Lister, M. L., & Savolainen, T. 2009, A&A, 507, L33
Quirrenbach, A., et al. 2000, A&AS, 141, 221
Raiteri, C. M., Villata, M., Capetti, A., Heidt, J., Arnaboldi, M., & Magazzù, A. 2007, A&A, 464, 871
Ransom, S. M., et al. 2011, ApJ, 727, L16
Rector, T. A., & Stocke, J. T. 2001, AJ, 122, 565

Richards, J. L., et al. 2011, ApJS, 194, 29
Rolke, W. A., López, A. M., & Conrad, J. 2005, Nuclear Instruments and Methods in Physics Research A, 551, 493
Rossetti, A., Mantovani, F., Dallacasa, D., Fanti, C., & Fanti, R. 2005, A&A, 434, 449
Rüger, M., Spanier, F., & Mannheim, K. 2010, MNRAS, 401, 973
Savage, A., Browne, I. W. A., & Bolton, J. G. 1976, MNRAS, 177, 77P
Savolainen, T., Homan, D. C., Hovatta, T., Kadler, M., Kovalev, Y. Y., Lister, M. L., Ros, E., & Zensus, J. A. 2010, A&A, 512, A24
Sbarufatti, B., Ciprini, S., Kotilainen, J., Decarli, R., Treves, A., Veronesi, A., & Falomo, R. 2009, AJ, 137, 337
Sbarufatti, B., Treves, A., & Falomo, R. 2005, ApJ, 635, 173
Sbarufatti, B., Treves, A., Falomo, R., Heidt, J., Kotilainen, J., & Scarpa, R. 2006, AJ, 132, 1
Scarpa, R., & Falomo, R. 1997, A&A, 325, 109
Schachter, J. F., et al. 1993, ApJ, 412, 541
Schinzel, F. K., Lobanov, A. P., Jorstad, S. G., Marscher, A. P., Taylor, G. B., & Zensus, J. A. 2010, ArXiv e-prints,1012.2820
Schmidt, M. 1977, ApJ, 217, 358
Schneider, D. P., et al. 2010, AJ, 139, 2360
Searle, L., & Bolton, J. G. 1968, ApJ, 154, L101
Shaw, M. S., Romani, R. W., Healey, S. E., Cotter, G., Michelson, P. F., & Readhead, A. C. S. 2009, ApJ, 704, 477
Shaw et al., M. 2011, in preparation
Smith, H. E., Burbidge, E. M., Baldwin, J. A., Tohline, J. E., Wampler, E. J., Hazard, C., & Murdoch, H. S. 1977, ApJ, 215, 427
Smith, R. J., Lucey, J. R., Hudson, M. J., Schlegel, D. J., & Davies, R. L. 2000, MNRAS, 313, 469
Sokolovsky, K. V., Kovalev, Y. Y., Pushkarev, A. B., & Lobanov, A. P. 2011, ArXiv e-prints
Sowards-Emmerd, D., Romani, R. W., Michelson, P. F., Healey, S. E., & Nolan, P. L. 2005, ApJ, 626, 95
Steidel, C. C., & Sargent, W. L. W. 1991, ApJ, 382, 433
Stickel, M., Fried, J. W., & Kuehr, H. 1988, A&A, 191, L16
—. 1989, A&AS, 80, 103
—. 1993a, A&AS, 98, 393
Stickel, M., & Kuehr, H. 1993, A&AS, 100, 395
Stickel, M., Kuehr, H., & Fried, J. W. 1993b, A&AS, 97, 483
Stickel, M., Meisenheimer, K., & Kuehr, H. 1994, A&AS, 105, 211
Strauss, M. A., Huchra, J. P., Davis, M., Yahil, A., Fisher, K. B., & Tonry, J. 1992, ApJS, 83, 29
Tadhunter, C. N., Morganti, R., di Serego-Alighieri, S., Fosbury, R. A. E., & Danziger, I. J. 1993, MNRAS, 263, 999
Tavecchio, F., & Ghiselini, G. 2008, MNRAS, 385, L98
Tavecchio, F., Ghiselini, G., Ghirlanda, G., Foschini, L., & Maraschi, L. 2010, MNRAS, 401, 1570
Taylor, G. B., et al. 2007, ApJ, 671, 1355
Thompson, D. J., Djorgovski, S., & de Carvalho, R. 1990, PASP, 102, 1235
Tingay, S. J., et al. 2001, ApJ, 549, L55
Ulrich, M.-H., Kinman, T. D., Lynds, C. R., Rieke, G. H., & Ekers, R. D. 1975, ApJ, 198, 261
Urry, C. M., & Padovani, P. 1995, PASP, 107, 803
Valtaoja, E., Lähteenmaki, A., & Terasranta, H. 1992, A&AS, 95, 73
Vermeulen, R. C., Ogle, P. M., Tran, H. D., Browne, I. W. A., Cohen, M. H., Readhead, A. C. S., Taylor, G. B., & Goodrich, R. W. 1995, ApJ, 452, L5
Véron-Cetty, M. P., & Véron, P. 2000, A&A Rev., 10, 81
Walsh, D., Beckers, J. M., Carswell, R. F., & Weymann, R. J. 1984, MNRAS, 211, 105
Walsh, D., & Carswell, R. F. 1982, MNRAS, 200, 191
Wehrle, A. E., Cohen, M. H., Unwin, S. C., Aller, H. D., Aller, M. F., & Nicolson, G. 1992, ApJ, 391, 589
White, G. L., Jauncey, D. L., Wright, A. E., Batty, M. J., Savage, A., Peterson, B. A., & Gulkis, S. 1988, ApJ, 327, 561
White, R. L., et al. 2000, ApJS, 126, 133
Wilkes, B. J. 1986, MNRAS, 218, 331
Wilkes, B. J., Wright, A. E., Jauncey, D. L., & Peterson, B. A. 1983, Proceedings of the Astronomical Society of Australia, 5, 2
Wills, D., & Lynds, R. 1978, ApJS, 36, 317
Wills, D., & Wills, B. J. 1974, ApJ, 190, 271
—. 1976, ApJS, 31, 143
Wright, A. E., Ables, J. G., & Allen, D. A. 1983, MNRAS, 205, 793
Xu, W., Lawrence, C. R., Readhead, A. C. S., & Pearson, T. J. 1994, AJ, 108, 395

Table 2
General Properties of AGNs in the Combined γ-ray and Radio Samples

J2000 (1)	B1950 (2)	1FGL Name (3)	Alias (4)	z (5)	Ref. (6)	Opt. (7)	SED (8)	Ref. (9)	Sample (10)
J0006−0623	0003−066	⋯	NRAO 005	0.3467	Jones et al. (2009)	B	LSP	1	R
J0017−0512	0015−054	J0017.4−0510	PMN J0017−0512	0.226	Shaw et al. (2011)	Q	LSP	2	G
J0050−0929	0048−097	J0050.6−0928	PKS 0048−09	⋯	⋯	B	ISP	2	B
J0108+0135	0106+013	J0108.6+0135	4C +01.02	2.099	Hewett et al. (1995)	Q	ISP	1	B

Table 2 — *Continued*

J2000 (1)	B1950 (2)	1FGL Name (3)	Alias (4)	z (5)	Ref. (6)	Opt. (7)	SED (8)	Ref. (9)	Sample (10)
J0112+2244	0109+224	J0112.0+2247	S2 0109+22	0.265	Healey et al. (2008)	B	ISP	1	G
J0112+3208	0110+318	J0112.9+3207	4C +31.03	0.603	Wills & Wills (1976)	Q	LSP	11	G
J0118−2141	0116−219	J0118.7−2137	OC -228	1.165	Wright et al. (1983)	Q	LSP	2	G
J0120−2701	0118−272	J0120.5−2700	OC -230.4	⋯	⋯	B	LSP	2	G
J0121+1149	0119+115	⋯	PKS 0119+11	0.570	Stickel et al. (1994)	Q	LSP	1	R
J0132−1654	0130−171	J0132.6−1655	OC -150	1.020	Wright et al. (1983)	Q	LSP	11	B
J0136+3905	0133+388	J0136.5+3905	B3 0133+388	⋯	⋯	B	HSP	5	G
J0136+4751	0133+476	J0137.0+4751	DA 55	0.859	Lawrence et al. (1996)	Q	LSP	1	B
J0145−2733	0142−278	J0144.9−2732	OC -270	1.148	Baker et al. (1999)	Q	LSP	2	G
J0205+3212	0202+319	J0205.3+3217	B2 0202+31	1.466	Burbidge (1970)	Q	LSP	1	R
J0204−1701	0202−172	J0205.0−1702	PKS 0202−17	1.739	Jones et al. (2009)	Q	LSP	2	R
J0217+7349	0212+735	J0217.8+7353	S5 0212+73	2.367	Lawrence et al. (1996)	Q	LSP	1	R
J0217+0144	0215+015	J0217.9+0144	OD 026	1.715	Boisse & Bergeron (1988)	Q	LSP	1	B
J0222+4302	0219+428	J0222.6+4302	3C 66A	⋯	⋯	B	HSP	5	G
J0231+1322	0229+131	⋯	4C +13.14	2.059	Osmer et al. (1994)	Q	LSP	6	R
J0237+2848	0234+285	J0237.9+2848	4C 28.07	1.206	Shaw et al. (2011)	Q	LSP	1	B
J0238+1636	0235+164	J0238.6+1637	AO 0235+164	0.940	Cohen et al. (1987)	Q	LSP	1	B
J0252−2219	0250−225	J0252.8−2219	OD -283	1.419	Shaw et al. (2011)	Q	LSP	11	G
J0303−2407	0301−243	J0303.5−2406	PKS 0301−243	0.260	Falomo & Ulrich (2000)	B	HSP	2	G
J0316+0904	0313+085	J0316.1+0904	BZB J0316+0904	⋯	⋯	B	HSP	5	G
J0319+4130	0316+413	J0319.7+4130	3C 84	0.0176	Strauss et al. (1992)	G	LSP	4	B
J0339−0146	0336−019	J0339.2−0143	CTA 26	0.852	Wills & Lynds (1978)	Q	LSP	1	R
J0349−2102	0347−211	J0349.9−2104	OE -280	2.944	Ellison et al. (2001)	Q	LSP	2	G
J0403+2600	0400+258	⋯	CTD 026	2.109	Schmidt (1977)	Q	⋯	⋯	R
J0423−0120	0420−014	J0423.2−0118	PKS 0420−01	0.9161	Jones et al. (2009)	Q	LSP	1	B
J0433+0521	0430+052	⋯	3C 120	0.033	Michel & Huchra (1988)	G	LSP	1	R
J0433+2905	0430+289	J0433.5+2905	BZB J0433+2905	⋯	⋯	B	ISP	5	G
J0442−0017	0440−003	J0442.7−0019	NRAO 190	0.844	Schmidt (1977)	Q	LSP	6	G
J0453−2807	0451−282	J0453.2−2805	OF -285	2.559	Wright et al. (1983)	Q	LSP	4	B
J0457−2324	0454−234	J0457.0−2325	PKS 0454−234	1.003	Stickel et al. (1989)	Q	LSP	2	B
J0507+6737	0502+675	J0507.9+6738	1ES 0502+675	0.416	Landt et al. (2002)	B	HSP	2	G
J0509+0541	0506+056	J0509.3+0540	TXS 0506+056	⋯	⋯	B	HSP	5	G
J0530+1331	0528+134	J0531.0+1331	PKS 0528+134	2.070	Hunter et al. (1993)	Q	LSP	1	B
J0532+0732	0529+075	J0532.9+0733	OG 050	1.254	Sowards-Emmerd et al. (2005)	Q	LSP	1	B
J0608−1520	0605−153	J0608.0−1521	PMN J0608−1520	1.094	Shaw et al. (2011)	Q	LSP	11	G
J0609−1542	0607−157	⋯	PKS 0607−15	0.3226	Jones et al. (2009)	Q	LSP	1	R
J0612+4122	0609+413	J0612.7+4120	B3 0609+413	⋯	⋯	B	⋯	⋯	G
J0630−2406	0628−240	J0630.9−2406	TXS 0628−240	⋯	⋯	B	ISP	4	G
J0646+4451	0642+449	⋯	OH 471	3.396	Osmer et al. (1994)	Q	LSP	1	R
J0654+4514	0650+453	J0654.3+4514	B3 0650+453	0.928	Shaw et al. (2011)	Q	LSP	2	G
J0654+5042	0650+507	J0654.4+5042	GB6 J0654+5042	1.253	Shaw et al. (2011)	Q	LSP	11	G
J0713+1935	0710+196	J0714.0+1935	WB92 0711+1940	0.540	Shaw et al. (2011)	Q	LSP	11	G
J0719+3307	0716+332	J0719.3+3306	B2 0716+33	0.779	White et al. (2000)	Q	LSP	2	G
J0721+7120	0716+714	J0721.9+7120	S5 0716+71	0.310	Nilsson et al. (2008)	B	ISP	5	B
J0738+1742	0735+178	J0738.2+1741	OI 158	⋯	⋯	B	LSP	1	G
J0739+0137	0736+017	J0739.1+0138	OI 061	0.1894	Ho & Kim (2009)	Q	ISP	1	B
J0748+2400	0745+241	⋯	PKS 0745+241	0.4092	Abazajian et al. (2005)	Q	LSP	4	R
J0750+1231	0748+126	J0750.6+1235	OI 280	0.889	Peterson et al. (1979)	Q	LSP	1	R
J0808−0751	0805−077	J0808.2−0750	PKS 0805−07	1.837	White et al. (1988)	Q	LSP	4	B
J0818+4222	0814+425	J0818.2+4222	OJ 425	⋯	⋯	B	LSP	1	B
J0825+0309	0823+033	J0825.9+0309	PKS 0823+033	0.506	Stickel et al. (1993a)	B	LSP	1	R
J0830+2410	0827+243	J0830.5+2407	OJ 248	0.942	Shaw et al. (2011)	Q	LSP	1	R
J0836−2016	0834−201	⋯	PKS 0834−20	2.752	Fricke et al. (1983)	Q	⋯	⋯	R
J0841+7053	0836+710	J0842.2+7054	4C 71.07	2.218	McIntosh et al. (1999)	Q	LSP	1	R
J0854+2006	0851+202	J0854.8+2006	OJ 287	0.306	Stickel et al. (1989)	B	LSP	1	B
J0909+0121	0906+015	J0909.0+0126	4C +01.24	1.0256	Shaw et al. (2011)	Q	ISP	1	B
J0920+4441	0917+449	J0920.9+4441	S4 0917+44	2.189	Abazajian et al. (2004)	Q	LSP	6	B
J0927+3902	0923+392	⋯	4C +39.25	0.695	Abazajian et al. (2005)	Q	LSP	1	R
J0948+4039	0945+408	⋯	4C +40.24	1.249	Abazajian et al. (2005)	Q	LSP	1	R
J0948+0022	0946+006	J0949.0+0021	PMN J0948+0022	0.585	Abazajian et al. (2004)	Q	LSP	2	G
J0957+5522	0954+556	J0957.7+5523	4C +55.17	0.8993	Shaw et al. (2011)	Q	LSP	6	G
J0958+6533	0954+658	J1000.1+6539	S4 0954+65	0.367	Rector & Stocke (2001)	B	LSP	5	R
J1012+2439	1009+245	J1012.7+2440	GB6 J1012+2439	1.805	Shaw et al. (2011)	Q	⋯	⋯	G
J1015+4926	1011+496	J1015.1+4927	7C 1011+4941	0.212	Albert et al. (2007)	B	HSP	2	G
J1016+0513	1013+054	J1016.1+0514	TXS 1013+054	1.713	Abazajian et al. (2004)	Q	⋯	⋯	G
J1037+5711	1034+574	J1037.7+5711	GB6 J1037+5711	⋯	⋯	B	ISP	5	G
J1037−2934	1034−293	⋯	PKS 1034−293	0.312	Scarpa & Falomo (1997)	Q	LSP	10	R
J1038+0512	1036+054	⋯	PKS 1036+054	0.473	Healey et al. (2008)	Q	LSP	1	R
J1058+0133	1055+018	J1058.4+0134	4C +01.28	0.888	Shaw et al. (2011)	Q	LSP	1	B
J1058+5628	1055+567	J1058.6+5628	7C 1055+5644	0.143	Abazajian et al. (2004)	B	HSP	5	G
J1104+3812	1101+384	J1104.4+3812	Mrk 421	0.0308	Ulrich et al. (1975)	B	HSP	2	G
J1121−0553	1118−056	J1121.5−0554	PKS 1118−05	1.297	Drinkwater et al. (1997)	Q	LSP	11	G
J1127−1857	1124−186	J1126.8−1854	PKS 1124−186	1.048	Drinkwater et al. (1997)	Q	ISP	1	R
J1130−1449	1127−145	J1130.2−1447	PKS 1127−14	1.184	Wilkes (1986)	Q	LSP	2	B
J1159+2914	1156+295	J1159.4+2914	4C +29.45	0.7246	Shaw et al. (2011)	Q	ISP	1	B
J1215−1731	1213−172	⋯	PKS 1213−17	⋯	⋯	U	LSP	1	R

Table 2 — *Continued*

J2000 (1)	B1950 (2)	1FGL Name (3)	Alias (4)	z (5)	Ref. (6)	Opt. (7)	SED (8)	Ref. (9)	Sample (10)
J1217+3007	1215+303	J1217.7+3007	ON 325	0.130	Akiyama et al. (2003)	B	HSP	5	G
J1221+3010	1218+304	J1221.3+3008	B2 1218+30	0.1836	Adelman-McCarthy et al. (2008)	B	HSP	9	G
J1221+2813	1219+285	J1221.5+2814	W Comae	⋯	⋯	B	ISP	5	G
J1224+2122	1222+216	J1224.7+2121	4C +21.35	0.434	Schneider et al. (2010)	Q	LSP	6	G
J1229+0203	1226+023	J1229.1+0203	3C 273	0.1583	Strauss et al. (1992)	Q	LSP	1	B
J1230+1223	1228+126	J1230.8+1223	M87	0.00436	Smith et al. (2000)	G	LSP	7	R
J1239+0443	1236+049	J1239.5+0443	BZQ J1239+0443	1.761	Shaw et al. (2011)	Q	LSP	11	G
J1246−2547	1244−255	J1246.7−2545	PKS 1244−255	0.633	Savage et al. (1976)	Q	LSP	2	G
J1248+5820	1246+586	J1248.2+5820	PG 1246+586	⋯	⋯	B	HSP	5	G
J1256−0547	1253−055	J1256.2−0547	3C 279	0.536	Marziani et al. (1996)	Q	LSP	1	B
J1303+2433	1300+248	J1303.0+2433	VIPS 0623	⋯	⋯	B	⋯	⋯	G
J1310+3220	1308+326	J1310.6+3222	OP 313	0.9973	Shaw et al. (2011)	Q	ISP	1	B
J1332−0509	1329−049	J1331.9−0506	OP −050	2.150	Thompson et al. (1990)	Q	LSP	2	G
J1332−1256	1329−126	J1332.6−1255	PMN J1332−1256	1.492	Shaw et al. (2011)	Q	⋯	⋯	G
J1337−1257	1334−127	J1337.7−1255	PKS 1335−127	0.539	Stickel et al. (1993b)	Q	LSP	1	B
J1344−1723	1341−171	J1344.2−1723	PMN J1344−1723	2.506	Shaw et al. (2011)	Q	⋯	⋯	G
J1427+2348	1424+240	J1426.9+2347	OQ +240	⋯	⋯	B	HSP	5	G
J1436+6336	1435+638	⋯	VIPS 0792	2.066	McIntosh et al. (1999)	Q	LSP	4	R
J1504+1029	1502+106	J1504.4+1029	OR 103	1.8385	Adelman-McCarthy et al. (2008)	Q	LSP	1	B
J1512−0905	1510−089	J1512.8−0906	PKS 1510−08	0.360	Thompson et al. (1990)	Q	LSP	1	B
J1516+1932	1514+197	J1516.9+1928	PKS 1514+197	⋯	⋯	B	LSP	5	R
J1517−2422	1514−241	J1517.8−2423	AP Librae	0.049	Jones et al. (2009)	B	LSP	2	B
J1522+3144	1520+319	J1522.1+3143	B2 1520+31	1.484	Shaw et al. (2011)	Q	LSP	2	G
J1542+6129	1542+616	J1542.9+6129	GB6 J1542+6129	⋯	⋯	B	ISP	5	G
J1549+0237	1546+027	J1549.3+0235	PKS 1546+027	0.414	Abazajian et al. (2004)	Q	LSP	1	R
J1550+0527	1548+056	J1550.7+0527	4C +05.64	1.417	Shaw et al. (2011)	Q	LSP	1	R
J1553+1256	1551+130	J1553.4+1255	OR +186	1.308	Schneider et al. (2010)	Q	⋯	⋯	G
J1555+1111	1553+113	J1555.7+1111	PG 1553+113	⋯	⋯	B	HSP	5	G
J1613+3412	1611+343	J1613.5+3411	DA 406	1.40	Shaw et al. (2011)	Q	LSP	1	R
J1625−2527	1622−253	J1625.7−2524	PKS 1622−253	0.786	di Serego-Alighieri et al. (1994)	Q	LSP	2	B
J1635+3808	1633+382	J1635.0+3808	4C +38.41	1.813	Shaw et al. (2011)	Q	LSP	1	B
J1638+5720	1637+574	⋯	OS 562	0.751	Marziani et al. (1996)	Q	ISP	1	R
J1640+3946	1638+398	⋯	NRAO 512	1.666	Stickel et al. (1989)	Q	LSP	1	R
J1642+3948	1641+399	J1642.5+3947	3C 345	0.593	Marziani et al. (1996)	Q	ISP	1	B
J1642+6856	1642+690	⋯	4C +69.21	0.751	Lawrence et al. (1996)	Q	LSP	6	R
J1653+3945	1652+398	J1653.9+3945	Mrk 501	0.0337	Stickel et al. (1993a)	B	HSP	2	G
J1658+0741	1655+077	⋯	PKS 1655+077	0.621	Wilkes (1986)	Q	LSP	1	R
J1700+6830	1700+685	J1700.1+6830	TXS 1700+685	0.301	Henstock et al. (1997)	Q	LSP	4	G
J1719+1745	1717+178	J1719.2+1745	OT 129	0.137	Sowards-Emmerd et al. (2005)	B	LSP	5	G
J1725+1152	1722+119	J1725.0+1151	1H 1720+117	⋯	⋯	B	HSP	5	G
J1727+4530	1726+455	J1727.3+4525	S4 1726+45	0.717	Henstock et al. (1997)	Q	LSP	1	R
J1733−1304	1730−130	J1733.0−1308	NRAO 530	0.902	Junkkarinen (1984)	Q	LSP	1	B
J1734+3857	1732+389	J1734.4+3859	OT 355	0.975	Shaw et al. (2011)	Q	LSP	11	G
J1740+5211	1739+522	J1740.0+5209	4C +51.37	1.379	Walsh et al. (1984)	Q	LSP	1	G
J1743−0350	1741−038	⋯	PKS 1741−03	1.054	White et al. (1988)	Q	LSP	1	R
J1751+0939	1749+096	J1751.5+0937	4C +09.57	0.322	Stickel et al. (1988)	B	LSP	1	B
J1753+2848	1751+288	⋯	B2 1751+28	1.118	Healey et al. (2008)	Q	LSP	1	R
J1801+4404	1800+440	⋯	S4 1800+44	0.663	Walsh & Carswell (1982)	Q	ISP	1	R
J1800+7828	1803+784	J1800.4+7827	S5 1803+784	0.6797	Lawrence et al. (1996)	B	LSP	1	B
J1806+6949	1807+698	J1807.0+6945	3C 371	0.051	de Grijp et al. (1992)	B	ISP	1	B
J1824+5651	1823+568	J1824.0+5651	4C +56.27	0.664	Shaw et al. (2011)	B	LSP	1	B
J1829+4844	1828+487	J1829.8+4845	3C 380	0.692	Lawrence et al. (1996)	Q	LSP	4	R
J1842+6809	1842+681	⋯	GB6 J1842+6809	0.472	Xu et al. (1994)	Q	⋯	⋯	R
J1848+3219	1846+322	J1848.5+3224	B2 1846+32A	0.798	Sowards-Emmerd et al. (2005)	Q	LSP	2	G
J1849+6705	1849+670	J1849.3+6705	S4 1849+67	0.657	Stickel & Kuehr (1993)	Q	LSP	1	B
J1903+5540	1902+556	J1903.0+5539	TXS 1902+556	⋯	⋯	B	ISP	5	G
J1911−2006	1908−201	J1911.2−2007	PKS B1908−201	1.119	Halpern et al. (2003)	Q	LSP	2	B
J1923−2104	1920−211	J1923.5−2104	OV −235	0.874	Halpern et al. (2003)	Q	LSP	2	B
J1924−2914	1921−293	J1925.2−2919	PKS B1921−293	0.3526	Jones et al. (2009)	Q	LSP	10	R
J1927+7358	1928+738	⋯	4C +73.18	0.302	Marziani et al. (1996)	Q	ISP	1	R
J1954−1123	1951−115	J1954.8−1124	TXS 1951−115	0.683	Shaw et al. (2011)	Q	LSP	11	G
J1955+5131	1954+513	⋯	⋯	1.223	Lawrence et al. (1996)	Q	LSP	7	R
J2000−1748	1958−179	J2000.9−1749	PKS 1958−179	0.652	Abdo et al. (2010d)	Q	LSP	1	B
J1959+6508	1959+650	J2000.0+6508	1ES 1959+650	0.047	Schachter et al. (1993)	B	HSP	2	G
J2011−1546	2008−159	⋯	PKS 2008−159	1.180	Peterson et al. (1979)	Q	ISP	1	R
J2022+6136	2021+614	⋯	OW 637	0.227	Hewitt & Burbidge (1991)	G	LSP	1	R
J2025−0735	2022−077	J2025.6−0735	PKS 2023−07	1.388	Drinkwater et al. (1997)	Q	LSP	2	G
J2031+1219	2029+121	J2031.5+1219	PKS 2029+121	1.213	Shaw et al. (2011)	Q	LSP	11	R
J2123+0535	2121+053	⋯	PKS 2121+053	1.941	Steidel & Sargent (1991)	Q	ISP	1	R
J2131−1207	2128−123	⋯	PKS 2128−12	0.501	Searle & Bolton (1968)	Q	ISP	1	R
J2134−0153	2131−021	J2134.0−0203	4C−02.81	1.284	Abdo et al. (2010d)	Q	LSP	1	R
J2136+0041	2134+004	⋯	PKS 2134+004	1.932	Osmer et al. (1994)	Q	LSP	1	R
J2139+1423	2136+141	⋯	OX 161	2.427	Wills & Wills (1974)	Q	LSP	7	R
J2143+1743	2141+175	J2143.4+1742	OX 169	0.2107	Ho & Kim (2009)	Q	ISP	2	G
J2147+0929	2144+092	J2147.2+0929	PKS 2144+092	1.113	White et al. (1988)	Q	LSP	2	G
J2148+0657	2145+067	J2148.5+0654	4C +06.69	0.999	Steidel & Sargent (1991)	Q	LSP	1	R

Table 2 — *Continued*

J2000 (1)	B1950 (2)	1FGL Name (3)	Alias (4)	z (5)	Ref. (6)	Opt. (7)	SED (8)	Ref. (9)	Sample (10)
J2158−1501	2155−152	J2157.9−1503	PKS 2155−152	0.672	White et al. (1988)	Q	LSP	1	R
J2202+4216	2200+420	J2202.8+4216	BL Lac	0.0686	Vermeulen et al. (1995)	B	LSP	1	B
J2203+1725	2201+171	J2203.5+1726	PKS 2201+171	1.076	Smith et al. (1977)	Q	ISP	1	G
J2203+3145	2201+315	⋯	4C +31.63	0.2947	Marziani et al. (1996)	Q	ISP	1	R
J2218−0335	2216−038	⋯	PKS 2216−03	0.901	Lynds (1967)	Q	ISP	1	R
J2225−0457	2223−052	J2225.8−0457	3C 446	1.404	Wright et al. (1983)	Q	LSP	4	B
J2229−0832	2227−088	J2229.7−0832	PHL 5225	1.5595	Abazajian et al. (2004)	Q	LSP	1	B
J2232+1143	2230+114	J2232.5+1144	CTA 102	1.037	Falomo et al. (1994)	Q	ISP	1	B
J2236−1433	2233−148	J2236.4−1432	OY -156	⋯	⋯	B	LSP	11	G
J2236+2828	2234+282	J2236.2+2828	CTD 135	0.795	Jackson & Browne (1991)	Q	LSP	7	G
J2243+2021	2241+200	J2244.0+2021	RGB J2243+203	⋯	⋯	B	ISP	5	G
J2246−1206	2243−123	⋯	PKS 2243−123	0.632	Browne et al. (1975)	Q	ISP	1	R
J2250−2806	2247−283	J2250.8−2809	PMN J2250−2806	0.525	Shaw et al. (2011)	Q	LSP	11	G
J2253+1608	2251+158	J2253.9+1608	3C 454.3	0.859	Jackson & Browne (1991)	Q	ISP	1	B
J2327+0940	2325+093	J2327.7+0943	OZ 042	1.841	Shaw et al. (2011)	Q	LSP	2	B
J2331−2148	2328−221	J2331.0−2145	PMN J2331−2148	0.563	Shaw et al. (2011)	Q	⋯	⋯	G
J2348−1631	2345−167	J2348.0−1629	PKS 2345−16	0.576	Tadhunter et al. (1993)	Q	LSP	1	R

Note. — Columns are as follows: (1) IAU name (J2000), (2) IAU name (B1950), (3) 1FGL catalog name, (4) other name, (5) redshift, (6) literature reference for redshift, (7) optical classification, where B = BL Lac, Q=Quasar, G = Radio galaxy, and U = Unidentified, (8) spectral energy distribution class, where HSP = high spectral peaked, ISP = intermediate spectral peaked, and LSP = low spectral peaked. (9) literature reference for SED data, where 1 = Chang (2010), 2 = Abdo et al. (2010e), 3 = Abdo et al. (2010a), 4 = Meyer et al., 2011, ApJ, submitted, 5 = Nieppola et al. (2006), 6 = Nieppola et al. (2008), 7 = Aatrokoski (2011), 8 = Tavecchio et al. (2010), 9 = Rüger et al. (2010), 10 = Impey & Neugebauer (1988), 11 = 2LAC catalog, Abdo et al., in preparation, (10) Sample membership, where G=1FM γ-ray selected sample, R = 1FM-matching radio sample, B = in both samples.

Table 3
Flux Data

J2000 Name (1)	B1950 Name (2)	VLBA Epoch (3)	VLBA Total (Jy) (4)	Single Dish Median (Jy) (5)	Arcsecond Emission (Jy) (6)	G_r (7)
J0006−0623	0003−066	2009 May 2	2.50	2.41	⋯	< 6.7
J0017−0512	0015−054	2009 Jul 5	0.29	0.32	⋯	972
J0050−0929	0048−097	2008 Oct 3	1.09	1.34	⋯	344
J0108+0135	0106+013	2009 Jun 25	2.77	2.66	⋯	1174
J0112+2244	0109+224	2009 Jul 5	0.48	0.79	⋯	489
J0112+3208	0110+318	2009 Jun 3	0.70	⋯	⋯	1332
J0118−2141	0116−219	2009 Jul 23	0.70	⋯	⋯	1047
J0120−2701	0118−272	2009 Dec 26	0.56	⋯	⋯	529
J0121+1149	0119+115	2009 Jun 15	3.57	3.76	⋯	< 9.9
J0132−1654	0130−171	2009 Oct 27	2.02	2.02	⋯	352
J0136+3906	0133+388	2010 Nov 29	0.05	⋯	⋯	9763
J0136+4751	0133+476	2009 Jun 25	4.44	3.87	⋯	415
J0145−2733	0142−278	2009 Dec 26	0.95	⋯	⋯	972
J0205+3212	0202+319	2008 Aug 25	3.17	3.26	⋯	106
J0204−1701	0202−172	2009 Jul 5	1.45	1.47	⋯	370
J0217+7349	0212+735	2008 Sep 12	3.78	3.72	⋯	296
J0217+0144	0215+015	2008 Nov 19	2.00	1.53	⋯	788
J0222+4302	0219+428	2009 Jun 15	0.60	0.86	0.25	3827
J0231+1322	0229+131	2010 Oct 25	1.90	1.57	⋯	< 51
J0237+2848	0234+285	2009 Jun 25	2.54	3.14	⋯	427
J0238+1636	0235+164	2009 Mar 25	3.08	3.15	⋯	1396
J0252−2219	0250−225	2009 Mar 25	0.51	⋯	⋯	2677
J0303−2407	0301−243	2010 Mar 1	0.21	⋯	⋯	1933
J0316+0904	0313+085	2010 Nov 20	0.06	⋯	⋯	4960
J0319+4130	0316+413	2009 May 28	19.40	18.91	⋯	63
J0339−0146	0336−019	2009 May 2	2.36	2.35	⋯	104
J0349−2102	0347−211	2009 Jul 5	0.62	⋯	⋯	3981
J0403+2600	0400+258	2010 Oct 15	1.85	1.85	⋯	< 75
J0423−0120	0420−014	2009 Jul 5	6.29	4.45	⋯	254
J0433+0521	0430+052	2009 Jul 5	2.69	3.18	0.56	< 27
J0433+2905	0430+289	2009 Jul 23	0.31	0.30	⋯	1280
J0442−0017	0440−003	2009 May 28	1.26	1.24	⋯	1050
J0453−2807	0451−282	2009 Aug 19	1.71	⋯	⋯	1201
J0457−2324	0454−234	2009 Jun 25	1.99	1.89[a]	⋯	2566
J0507+6737	0502+675	2010 Nov 20	0.05	0.03	⋯	9048
J0509+0541	0506+056	2009 Jun 3	0.59	0.60	⋯	646
J0530+1331	0528+134	2009 Mar 25	2.86	2.98	⋯	838
J0532+0732	0529+075	2009 May 2	1.47	1.42	⋯	608
J0608−1520	0605−153	2010 Mar 1	0.20	0.21	⋯	4471
J0609−1542	0607−157	2009 Jun 25	5.17	4.92	⋯	< 12
J0612+4122	0609+413	2009 Dec 26	0.22	0.28	⋯	1022

Table 3 — *Continued*

J2000 Name	B1950 Name	VLBA Epoch	VLBA Total (Jy)	Single Dish Median (Jy)	Arcsecond Emission (Jy)	G_r
(1)	(2)	(3)	(4)	(5)	(6)	(7)
J0630−2406	0628−240	2010 Nov 29	0.07	· · ·	· · ·	4221
J0646+4451	0642+449	2009 May 28	3.62	3.43	· · ·	< 57
J0654+4514	0650+453	2009 Jun 25	0.38	0.50	· · ·	2063
J0654+5042	0650+507	2009 Jul 5	0.20	0.23	· · ·	2805
J0713+1935	0710+196	2009 Aug 19	0.44	· · ·	· · ·	1885
J0719+3307	0716+332	2009 Feb 25	0.57	0.58	· · ·	1193
J0721+7120	0716+714	2009 Jun 15	1.20	2.09	· · ·	534
J0738+1742	0735+178	2009 Jun 25	0.62	0.74	0.19	629
J0739+0137	0736+017	2009 Jul 5	1.20	1.33	0.20	328
J0748+2400	0745+241	2010 Oct 25	1.15	1.54	· · ·	< 16
J0750+1231	0748+126	2009 Feb 25	4.30	4.33	· · ·	70
J0808−0751	0805−077	2009 Jun 25	1.91	1.08	· · ·	1835
J0818+4222	0814+425	2009 May 28	1.68	1.44	· · ·	523
J0825+0309	0823+033	2009 Jul 5	0.98	1.53	· · ·	70
J0830+2410	0827+243	2008 Nov 19	1.53	1.49	· · ·	353
J0836−2016	0834−201	2009 Mar 25	2.07	· · ·	0.65	< 118
J0841+7053	0836+710	2009 May 2	1.58	1.57	· · ·	1028
J0854+2006	0851+202	2009 May 28	4.67	3.78	· · ·	88
J0909+0121	0906+015	2009 May 28	1.54	1.35	· · ·	781
J0920+4441	0917+449	2009 Jun 25	2.12	2.02	· · ·	2154
J0927+3902	0923+392	2009 Jul 5	10.86	10.18	· · ·	< 2.4
J0948+4039	0945+408	2009 Jun 3	1.69	1.76	· · ·	< 44
J0948+0022	0946+006	2009 May 28	0.44	0.24	· · ·	2901
J0957+5522	0954+556	2009 Mar 25	0.15	1.19	0.96	5909
J0958+6533	0954+658	2009 Jul 5	1.34	1.28	· · ·	74
J1012+2439	1009+245	2010 Nov 29	0.05	0.05	· · ·	14584
J1015+4926	1011+496	2009 May 2	0.20	0.28	0.08	3431
J1016+0513	1013+054	2009 Jun 15	0.66	0.62	· · ·	2730
J1037+5711	1034+574	2010 Mar 1	0.11	0.17	· · ·	1649
J1037−2934	1034−293	2010 Oct 15	1.44	· · ·	· · ·	< 13
J1038+0512	1036+054	2008 Oct 3	1.49	1.38	· · ·	< 17
J1058+0133	1055+018	2008 Aug 25	4.32	4.65	· · ·	265
J1058+5628	1055+567	2009 Aug 19	0.18	0.17	· · ·	3011
J1104+3812	1101+384	2009 Jun 25	0.33	0.44	0.11	6456
J1121−0553	1118−056	2009 Jun 15	0.48	· · ·	· · ·	1495
J1127−1857	1124−186	2009 May 2	1.74	1.64	· · ·	334
J1130−1449	1127−145	2009 Jul 5	2.33	2.27	· · ·	528
J1159+2914	1156+295	2009 Jun 3	2.18	3.07	· · ·	280
J1215−1731	1213−172	2008 Sep 12	1.75	1.80	0.16	< 41
J1217+3007	1215+303	2009 Jun 15	0.36	0.38	· · ·	1223
J1221+3010	1218+304	2010 Nov 20	0.07	· · ·	· · ·	4114
J1221+2813	1219+285	2009 May 28	0.33	0.40	0.07	1837
J1224+2122	1222+216	2009 May 28	1.01	1.15	0.13	359
J1229+0203	1226+023	2009 Jun 25	24.38	27.84	6.58	83
J1230+1223	1228+126	2009 Jul 5	2.51	26.30	23.71	45
J1239+0443	1236+049	2009 Jun 3	0.36	0.38	· · ·	2926
J1246−2547	1244−255	2009 Jun 15	1.10	· · ·	· · ·	970
J1248+5820	1246+586	2009 Oct 27	0.12	0.16	· · ·	2929
J1256−0547	1253−055	2009 Jun 25	12.01	13.65	· · ·	328
J1303+2433	1300+248	2010 Nov 13	0.11	0.28	· · ·	1049
J1310+3220	1308+326	2009 Jun 3	2.22	1.75	· · ·	705
J1332−0509	1329−049	2009 Jul 5	1.12	0.99	· · ·	3117
J1332−1256	1329−126	2010 Mar 1	0.35	· · ·	· · ·	3917
J1337−1257	1334−127	2009 Jun 25	6.59	6.51	· · ·	66
J1344−1723	1341−171	2009 Jun 25	0.33	0.39	· · ·	3486
J1427+2348	1424+240	2009 Jun 25	0.18	0.26	0.06	5450
J1436+6336	1435+638	2010 Jul 12	1.54	1.50	· · ·	< 41
J1504+1029	1502+106	2009 Mar 25	3.15	2.65	· · ·	5965
J1512−0905	1510−089	2009 Jul 5	3.98	2.75	· · ·	2335
J1516+1932	1514+197	2010 Sep 27	0.90	1.56	· · ·	64
J1517−2422	1514−241	2009 Jun 3	2.32	· · ·	· · ·	168
J1522+3144	1520+319	2009 Jun 15	0.42	0.40	· · ·	12312
J1542+6129	1542+616	2010 Nov 29	0.14	0.13	· · ·	3628
J1549+0237	1546+027	2009 Jun 25	1.79	1.72	· · ·	191
J1550+0527	1548+056	2009 Jan 30	2.64	2.83	· · ·	56
J1553+1256	1551+130	2009 Jun 3	0.67	0.67	· · ·	2032
J1555+1111	1553+113	2009 Jun 15	0.15	0.18	· · ·	8397
J1613+3412	1611+343	2009 May 2	2.81	2.83	· · ·	46
J1625−2527	1622−253	2009 Oct 27	2.32	· · ·	· · ·	286
J1635+3808	1633+382	2009 May 2	2.88	2.80	· · ·	933
J1638+5720	1637+574	2009 Mar 25	1.81	1.80	· · ·	< 13
J1640+3946	1638+398	2009 May 28	0.78	0.79	· · ·	< 418
J1642+3948	1641+399	2009 Jul 5	9.14	7.72	· · ·	130
J1642+6856	1642+690	2008 Nov 26	3.84	4.62	· · ·	< 7.3

Table 3 — *Continued*

J2000 Name (1)	B1950 Name (2)	VLBA Epoch (3)	VLBA Total (Jy) (4)	Single Dish Median (Jy) (5)	Arcsecond Emission (Jy) (6)	G_r (7)
J1653+3945	1652+398	2009 Jun 15	0.87	1.17	0.30	812
J1658+0741	1655+077	2009 Jul 5	1.85	· · ·	· · ·	< 29
J1700+6830	1700+685	2009 Jul 5	0.25	0.30	· · ·	1201
J1719+1745	1717+178	2009 Jul 5	0.58	0.58	· · ·	533
J1725+1152	1722+119	2010 Nov 20	0.07	0.07	· · ·	5390
J1727+4530	1726+455	2008 Aug 25	1.02	1.39	· · ·	215
J1733−1304	1730−130	2009 Jun 25	4.00	4.74	· · ·	113
J1734+3857	1732+389	2009 Dec 26	0.97	0.88	· · ·	1097
J1740+5211	1739+522	2008 Aug 25	0.94	1.16	· · ·	1504
J1743−0350	1741−038	2008 Nov 19	3.26	3.02	· · ·	< 33
J1751+0939	1749+096	2009 Jun 3	4.20	5.13	· · ·	136
J1753+2848	1751+288	2009 Jun 25	1.48	1.57	· · ·	< 44
J1801+4404	1800+440	2008 Aug 25	1.32	1.44	· · ·	< 52
J1800+7828	1803+784	2009 Mar 25	2.40	2.31	· · ·	212
J1806+6949	1807+698	2009 Jul 5	1.37	1.60	0.23	163
J1824+5651	1823+568	2009 May 28	1.59	1.61	· · ·	266
J1829+4844	1828+487	2009 Mar 25	1.80	2.81^a	1.27	56
J1842+6809	1842+681	2010 Oct 25	0.50	0.88	· · ·	< 59
J1848+3219	1846+322	2009 Jun 3	0.62	0.61	· · ·	1036
J1849+6705	1849+670	2008 Oct 3	1.88	2.60	· · ·	700
J1903+5540	1902+556	2010 Nov 20	0.18	0.11	· · ·	2464
J1911−2006	1908−201	2009 Jun 25	1.64	· · ·	· · ·	633
J1923−2104	1920−211	2009 Jun 15	2.06	· · ·	· · ·	786
J1924−2914	1921−293	2010 Mar 1	15.54	14.16^a	· · ·	18
J1927+7358	1928+738	2009 May 28	3.71	3.21	· · ·	< 13
J1954−1123	1951−115	2009 Dec 26	0.42	0.32	· · ·	1705
J1955+5131	1954+513	2010 Oct 15	1.26	1.52	· · ·	< 21
J2000−1748	1958−179	2009 Jul 5	2.85	2.54	· · ·	221
J1959+6508	1959+650	2009 Jun 3	0.22	0.21	0.03	3021
J2011−1546	2008−159	2008 Aug 25	2.04	1.99	· · ·	< 64
J2022+6136	2021+614	2009 Jan 30	2.26	2.31	· · ·	< 11
J2025−0735	2022−077	2009 Jun 15	0.95	1.11	· · ·	2978
J2031+1219	2029+121	2010 Oct 15	1.26	1.36	· · ·	262
J2123+0535	2121+053	2009 May 28	1.92	1.65	· · ·	< 81
J2131−1207	2128−123	2009 Jan 7	2.23	2.27	· · ·	< 18
J2134−0153	2131−021	2009 Feb 25	2.41	2.31	· · ·	54
J2136+0041	2134+004	2008 Nov 19	6.67	6.53	· · ·	< 14
J2139+1423	2136+141	2009 Jul 5	2.71	2.53	· · ·	< 32
J2143+1743	2141+175	2009 Jun 3	1.09	0.81	· · ·	816
J2147+0929	2144+092	2009 Jun 25	1.30	0.83	· · ·	1878
J2148+0657	2145+067	2009 Mar 25	5.57	5.54	· · ·	38
J2158−1501	2155−152	2009 May 2	1.69	1.61	· · ·	90
J2202+4216	2200+420	2009 Jun 15	4.52	3.23	· · ·	180
J2203+1725	2201+171	2009 Jul 5	1.16	1.07	· · ·	889
J2203+3145	2201+315	2009 Feb 25	2.60	2.57	· · ·	< 5.3
J2218−0335	2216−038	2009 Mar 25	1.50	1.60	· · ·	< 14
J2225−0457	2223−052	2009 May 2	7.51	8.05	· · ·	96
J2229−0832	2227−088	2009 Jun 3	2.75	2.62	· · ·	973
J2232+1143	2230+114	2009 Mar 25	3.87	5.23	· · ·	238
J2236−1433	2233−148	2009 Dec 26	0.52	0.45	· · ·	672
J2236+2828	2234+282	2009 Dec 26	1.21	1.22	· · ·	607
J2243+2021	2241+200	2010 Nov 29	0.07	0.07	· · ·	5133
J2246−1206	2243−123	2009 Jun 15	2.19	2.18	· · ·	< 23
J2250−2806	2247−283	2009 Jun 3	0.51	· · ·	· · ·	781
J2253+1608	2251+158	2009 Jun 25	6.83	12.74	· · ·	788
J2327+0940	2325+093	2009 Jun 15	2.01	2.44	· · ·	1092
J2331−2148	2328−221	2010 Nov 29	0.14	· · ·	· · ·	3278
J2348−1631	2345−167	2009 May 2	2.23	2.04	· · ·	120

Note. — Columns are as follows: (1) IAU name (J2000), (2) IAU name (B1950), (3) VLBA observation date, (4) total 15 GHz VLBA flux density in Jy, (5) single dish OVRO 15 GHz median flux density in Jy during 11 month Fermi era. The *a* flag indicates UMRAO 14.5 GHz data, (6) arcsecond scale 15 GHz flux density in Jy, (7) ratio of average > 100 MeV γ-ray energy luminosity to 15 GHz radio luminosity.

Table 4
Jet Data

J2000 Name (1)	B1950 Name (2)	Op. Angle (deg) (3)	Jet P.A. (deg) (4)	Core T_b (K) (5)	m (%) (6)	Core EVPA (deg) (7)
J0006−0623	0003−066	22	−95	> 12.8	7.8	15

Table 4 — *Continued*

J2000 Name	B1950 Name	Op. Angle (deg)	Jet P.A. (deg)	Core T_b (K)	m (%)	Core EVPA (deg)
(1)	(2)	(3)	(4)	(5)	(6)	(7)
J0017−0512	0015−054	39	−123	11.4	< 0.3	⋯
J0050−0929	0048−097	15	−8	> 13.2	3.7	150
J0108+0135	0106+013	28	−127	12.6	0.9	113
J0112+2244	0109+224	22	86	11.3	1.5	68
J0112+3208	0110+318	18	−66	12.2	2.2	115
J0118−2141	0116−219	32	−69	11.2	1.1	122
J0120−2701	0118−272	13	−26	11.1	5.5	136
J0121+1149	0119+115	15	3	12.9	5.1	156
J0132−1654	0130−171	21	−109	12.1	2.5	0
J0136+3906	0133+388	⋯	⋯	> 10.6	⋯	⋯
J0136+4751	0133+476	21	−38	12.7	2.0	95
J0145−2733	0142−278	25	54	11.4	1.3	96
J0205+3212	0202+319	12	−11	12.3	3.5	108
J0204−1701	0202−172	15	7	12.5	3.7	93
J0217+7349	0212+735	12	113	> 13.9	1.3	42
J0217+0144	0215+015	47	108	12.6	3.2	4
J0222+4302	0219+428	20	171	12.0	2.9	25
J0231+1322	0229+131	27	64	> 13.5	4.1	179
J0237+2848	0234+285	23	−13	12.1	3.9	135
J0238+1636	0235+164	19	−34	12.0	0.5	8
J0252−2219	0250−225	68	−155	> 12.8	2.4	16
J0303−2407	0301−243	25	−125	10.7	1.0	50
J0316+0904	0313+085	21	24	10.5	⋯	⋯
J0319+4130	0316+413	30	−176	11.1	0.04	123
J0339−0146	0336−019	33	61	11.8	3.6	100
J0349−2102	0347−211	15	−147	12.7	1.8	31
J0403+2600	0400+258	13	77	11.2	4.0	130
J0423−0120	0420−014	24	−161	12.2	2.2	131
J0433+0521	0430+052	13	−115	> 12.0	< 0.2	⋯
J0433+2905	0430+289	54	56	11.3	2.6	41
J0442−0017	0440−003	42	−130	11.3	2.3	172
J0453−2807	0451−282	9	8	12.7	1.3	48
J0457−2324	0454−234	31	134	> 13.3	1.0	160
J0507+6737	0502+675	⋯	⋯	10.7	⋯	⋯
J0509+0541	0506+056	26	−173	11.1	1.1	139
J0530+1331	0528+134	20	52	12.1	2.7	166
J0532+0732	0529+075	50	−25	10.4	3.8	165
J0608−1520	0605−153	56	100	11.0	< 0.5	⋯
J0609−1542	0607−157	35	68	11.2	4.8	82
J0612+4122	0609+413	20	119	11.5	0.5	178
J0630−2406	0628−240	30	−151	10.5	⋯	⋯
J0646+4451	0642+449	21	83	12.5	1.6	164
J0654+4514	0650+453	46	97	11.9	0.5	42
J0654+5042	0650+507	20	93	10.8	5.0	101
J0713+1935	0710+196	42	87	11.9	1.4	108
J0719+3307	0716+332	22	76	12.1	1.8	99
J0721+7120	0716+714	18	18	12.7	2.3	154
J0738+1742	0735+178	23	63	11.3	1.6	129
J0739+0137	0736+017	21	−79	11.7	1.1	168
J0748+2400	0745+241	15	−59	11.9	2.0	85
J0750+1231	0748+126	23	89	12.1	2.6	35
J0808−0751	0805−077	20	−30	13.1	1.9	154
J0818+4222	0814+425	41	100	12.2	1.6	2
J0825+0309	0823+033	24	26	12.6	5.3	41
J0830+2410	0827+243	21	124	11.9	2.3	25
J0836−2016	0834−201	34	−100	10.4	1.6	136
J0841+7053	0836+710	10	−145	12.6	0.1	93
J0854+2006	0851+202	29	−115	12.4	5.9	156
J0909+0121	0906+015	19	43	12.2	2.5	130
J0920+4441	0917+449	17	178	12.7	3.7	119
J0927+3902	0923+392	16	101	10.6	< 0.7	⋯
J0948+4039	0945+408	17	116	12.1	2.1	3
J0948+0022	0946+006	21	24	> 12.8	0.8	142
J0957+5522	0954+556	⋯	⋯	8.5	6.9	9
J0958+6533	0954+658	30	−38	11.9	2.4	51
J1012+2439	1009+245	23	38	10.7	⋯	⋯
J1015+4926	1011+496	20	−105	11.3	1.1	134
J1016+0513	1013+054	28	140	12.2	2.5	97
J1037+5711	1034+574	⋯	−167	10.7	< 0.8	⋯
J1037−2934	1034−293	32	123	11.6	3.4	23
J1038+0512	1036+054	12	−5	12.6	6.8	154
J1058+0133	1055+018	28	−55	12.2	6.4	127
J1058+5628	1055+567	36	−85	10.7	< 0.5	⋯
J1104+3812	1101+384	27	−34	> 12.4	1.3	94

Table 4 — *Continued*

J2000 Name	B1950 Name	Op. Angle (deg)	Jet P.A. (deg)	Core T_b (K)	m (%)	Core EVPA (deg)
(1)	(2)	(3)	(4)	(5)	(6)	(7)
J1121−0553	1118−056	11	31	12.0	2.0	139
J1127−1857	1124−186	15	169	12.5	2.0	106
J1130−1449	1127−145	18	81	11.9	0.5	38
J1159+2914	1156+295	20	9	12.1	1.8	16
J1215−1731	1213−172	23	112	11.3	3.2	83
J1217+3007	1215+303	13	144	11.4	< 0.2	⋯
J1221+3010	1218+304	22	94	10.5	⋯	⋯
J1221+2813	1219+285	16	112	11.6	1.3	2
J1224+2122	1222+216	13	−2	11.8	6.4	8
J1229+0203	1226+023	12	−125	12.1	0.2	10
J1230+1223	1228+126	13	−73	10.9	0.1	0
J1239+0443	1236+049	29	−60	12.3	1.1	100
J1246−2547	1244−255	22	140	> 13.1	1.3	50
J1248+5820	1246+586	47	4	11.1	< 0.7	⋯
J1256−0547	1253−055	16	−124	12.9	2.0	65
J1303+2433	1300+248	⋯	−41	11.7	< 0.5	⋯
J1310+3220	1308+326	38	−59	12.2	1.4	77
J1332−0509	1329−049	14	18	12.7	< 0.07	⋯
J1332−1256	1329−126	25	112	> 12.5	0.7	87
J1337−1257	1334−127	19	149	12.6	4.3	169
J1344−1723	1341−171	53	−56	> 12.7	1.6	21
J1427+2348	1424+240	56	145	11.0	2.1	153
J1436+6336	1435+638	5	−127	10.7	< 0.5	⋯
J1504+1029	1502+106	43	116	13.1	1.3	164
J1512−0905	1510−089	19	−32	12.7	2.3	151
J1516+1932	1514+197	19	−24	12.6	2.3	168
J1517−2422	1514−241	10	161	11.1	0.6	91
J1522+3144	1520+319	63	14	11.4	1.4	59
J1542+6129	1542+616	14	109	11.4	1.8	139
J1549+0237	1546+027	16	175	> 13.3	2.8	46
J1550+0527	1548+056	14	−6	12.1	4.4	141
J1553+1256	1551+130	14	11	12.2	1.8	70
J1555+1111	1553+113	45	48	10.7	< 0.5	⋯
J1613+3412	1611+343	28	168	11.6	2.2	85
J1625−2527	1622−253	23	14	11.7	1.2	111
J1635+3808	1633+382	21	−79	12.8	0.5	101
J1638+5720	1637+574	14	−156	13.4	0.3	146
J1640+3946	1638+398	66	−77	11.5	0.8	141
J1642+3948	1641+399	16	−89	12.6	0.7	122
J1642+6856	1642+690	15	−167	12.7	4.9	104
J1653+3945	1652+398	28	128	11.0	0.5	105
J1658+0741	1655+077	15	−42	12.9	5.6	103
J1700+6830	1700+685	17	142	> 12.2	0.5	38
J1719+1745	1717+178	10	−157	11.8	9.4	31
J1725+1152	1722+119	⋯	⋯	> 10.7	⋯	⋯
J1727+4530	1726+455	26	−110	12.6	1.2	100
J1733−1304	1730−130	12	8	12.6	3.0	58
J1734+3857	1732+389	25	117	12.3	2.1	169
J1740+5211	1739+522	62	15	12.3	0.7	77
J1743−0350	1741−038	22	−161	11.7	2.6	149
J1751+0939	1749+096	28	17	12.7	4.1	7
J1753+2848	1751+288	22	9	> 13.1	0.9	18
J1801+4404	1800+440	22	−156	11.7	1.5	46
J1800+7828	1803+784	22	−90	12.1	2.5	77
J1806+6949	1807+698	10	−101	11.3	< 0.09	⋯
J1824+5651	1823+568	8	−160	12.5	6.8	14
J1829+4844	1828+487	15	−40	12.1	1.3	90
J1842+6809	1842+681	12	138	11.9	2.2	129
J1848+3219	1846+322	24	−41	> 13.2	1.7	144
J1849+6705	1849+670	18	−45	12.7	2.1	84
J1903+5540	1902+556	32	41	11.8	5.4	22
J1911−2006	1908−201	25	19	13.0	0.7	67
J1923−2104	1920−211	30	−8	13.4	1.0	134
J1924−2914	1921−293	36	17	12.2	3.0	131
J1927+7358	1928+738	9	162	12.0	0.10	178
J1954−1123	1951−115	27	10	11.8	6.4	123
J1955+5131	1954+513	19	−59	11.9	3.0	43
J2000−1748	1958−179	24	105	12.5	1.3	11
J1959+6508	1959+650	37	139	11.0	2.3	149
J2011−1546	2008−159	14	12	11.8	1.3	14
J2022+6136	2021+614	6	32	10.6	0.1	137
J2025−0735	2022−077	19	−13	12.2	2.3	128
J2031+1219	2029+121	19	−154	12.3	0.8	101
J2123+0535	2121+053	18	−97	11.9	8.1	25

M. L. Lister et al.

Table 4 — *Continued*

J2000 Name (1)	B1950 Name (2)	Op. Angle (deg) (3)	Jet P.A. (deg) (4)	Core T_b (K) (5)	m (%) (6)	Core EVPA (deg) (7)
J2131−1207	2128−123	11	−150	11.3	0.6	54
J2134−0153	2131−021	35	104	12.1	7.0	89
J2136+0041	2134+004	22	−84	12.4	1.9	22
J2139+1423	2136+141	31	−76	12.0	4.1	139
J2143+1743	2141+175	31	−52	11.7	1.0	90
J2147+0929	2144+092	37	78	12.7	2.0	11
J2148+0657	2145+067	27	118	11.8	0.5	40
J2158−1501	2155−152	18	−148	11.9	3.0	18
J2202+4216	2200+420	27	−171	12.1	8.1	13
J2203+1725	2201+171	21	49	12.5	0.9	135
J2203+3145	2201+315	15	−144	12.0	0.9	122
J2218−0335	2216−038	14	−172	11.2	1.2	157
J2225−0457	2223−052	24	98	12.5	2.5	33
J2229−0832	2227−088	15	−10	12.8	1.5	172
J2232+1143	2230+114	15	152	12.8	1.7	80
J2236−1433	2233−148	42	105	11.3	7.4	84
J2236+2828	2234+282	25	−135	10.8	4.8	36
J2243+2021	2241+200	7	9	10.7	⋯	⋯
J2246−1206	2243−123	14	8	12.0	2.3	124
J2250−2806	2247−283	20	159	> 12.6	2.0	23
J2253+1608	2251+158	48	−76	12.3	2.2	151
J2327+0940	2325+093	32	−96	12.6	1.6	91
J2331−2148	2328−221	13	153	11.4	< 0.4	⋯
J2348−1631	2345−167	28	124	12.5	2.5	41

Note. — Columns are as follows: (1) IAU name (J2000), (2) IAU name (B1950), (3) opening angle of the jet (degrees), (4) position angle of the parsec-scale jet (degrees), (5) log brightness temperature of the core (K), (6) fractional linear polarization of the core in per cent, (7) linear polarization electric vector position angle at the location of the core (degrees).